Northumbria Research Link

Citation: Kirillov, Oleg (2017) Singular diffusionless limits of double-diffusive instabilities in magnetohydrodynamics. Proceedings of the Royal Society A : Mathematical, Physical and Engineering Sciences, 473 (2205). ISSN 1364-5021

Published by: Royal Society

URL: https://doi.org/10.1098/rspa.2017.0344 <https://doi.org/10.1098/rspa.2017.0344>

This version was downloaded from Northumbria Research Link: http://nrl.northumbria.ac.uk/31129/

Northumbria University has developed Northumbria Research Link (NRL) to enable users to access the University's research output. Copyright © and moral rights for items on NRL are retained by the individual author(s) and/or other copyright owners. Single copies of full items can be reproduced, displayed or performed, and given to third parties in any format or medium for personal research or study, educational, or not-for-profit purposes without prior permission or charge, provided the authors, title and full bibliographic details are given, as well as a hyperlink and/or URL to the original metadata page. The content must not be changed in any way. Full items must not be sold commercially in any format or medium without formal permission of the copyright holder. The full policy is available online: http://nrl.northumbria.ac.uk/policies.html

This document may differ from the final, published version of the research and has been made available online in accordance with publisher policies. To read and/or cite from the published version of the research, please visit the publisher's website (a subscription may be required.)

www.northumbria.ac.uk/nrl

northumbria UNIVERSITY NEWCASTLE

Downloaded from http://rspa.royalsocietypublishing.org/ on September 13, 2017

PROCEEDINGS A

rspa.royalsocietypublishing.org

Research

Cite this article: Kirillov ON. 2017 Singular diffusionless limits of double-diffusive instabilities in magnetohydrodynamics. *Proc. R. Soc. A* **473**: 20170344.
http://dx.doi.org/10.1098/rspa.2017.0344

Received: 16 May 2017
Accepted: 15 August 2017

Subject Areas:
fluid mechanics, astrophysics, applied mathematics

Keywords:
Hamiltonian system, energy equipartition, double diffusion, magnetorotational instability, dissipation-induced instabilities, exceptional point

Author for correspondence:
Oleg N. Kirillov
e-mail: oleg.kirillov@northumbria.ac.uk
e-mail: kirillov@mi.ras.ru

Singular diffusionless limits of double-diffusive instabilities in magnetohydrodynamics

Oleg N. Kirillov[1,2]

[1]Northumbria University, Newcastle upon Tyne NE1 8ST, UK
[2]Steklov Mathematical Institute, Russian Academy of Sciences, Gubkina 8, Moscow 119991, Russia

ONK, 0000-0002-6150-9308

We study local instabilities of a differentially rotating viscous flow of electrically conducting incompressible fluid subject to an external azimuthal magnetic field. In the presence of the magnetic field, the hydrodynamically stable flow can demonstrate non-axisymmetric azimuthal magnetorotational instability (AMRI) both in the diffusionless case and in the double-diffusive case with viscous and ohmic dissipation. Performing stability analysis of amplitude transport equations of short-wavelength approximation, we find that the threshold of the diffusionless AMRI via the Hamilton–Hopf bifurcation is a singular limit of the thresholds of the viscous and resistive AMRI corresponding to the dissipative Hopf bifurcation and manifests itself as the Whitney umbrella singular point. A smooth transition between the two types of instabilities is possible only if the magnetic Prandtl number is equal to unity, $Pm = 1$. At a fixed $Pm \neq 1$, the threshold of the double-diffusive AMRI is displaced by finite distance in the parameter space with respect to the diffusionless case even in the zero dissipation limit. The complete neutral stability surface contains three Whitney umbrella singular points and two mutually orthogonal intervals of self-intersection. At these singularities, the double-diffusive system reduces to a marginally stable system which is either Hamiltonian or parity–time-symmetric.

Dedicated to the memory of Professor V. V. Beletsky.

THE ROYAL SOCIETY PUBLISHING

© 2017 The Authors. Published by the Royal Society under the terms of the Creative Commons Attribution License http://creativecommons.org/licenses/by/4.0/, which permits unrestricted use, provided the original author and source are credited.

Downloaded from http://rspa.royalsocietypublishing.org/ on September 13, 2017

1. Introduction

While common sense tends to assign to dissipation the role of a vibration damper, as early as 1879 Kelvin and Tait predicted viscosity-driven instability of Maclaurin's spheroids (proved by Roberts & Stewartson in 1963 [1–3]), thus presenting a class of Hamiltonian equilibria, which, although stable in the absence of dissipation, become unstable due to the action of dissipative forces [4,5]. The universality of the *dissipation-induced instabilities* manifests itself in unexpected links between solid- and fluid mechanics [6–8]. For instance, the destabilizing action of viscous dissipation on the negative energy mode of rotation of a particle moving in a rotating cavity [9] selects backward whirling in the rotating frame as an unstable (anticyclonic) motion. Remarkably, this very instability mechanism described by Lamb in 1908 has recently reappeared as a trigger breaking the cyclone–anticyclone vortex symmetry in a rotating fluid in the presence of linear Ekman friction [10].

The onset of the classical Hopf bifurcation in a near-Hamiltonian dissipative system generically does not converge to the onset of the Hamilton–Hopf bifurcation of a Hamiltonian system when dissipation tends to zero [11]. For instance, the onset of secular instability (classical Hopf) of viscous Maclaurin spheroids does not tend to the onset of dynamical instability (Hamilton–Hopf) of inviscid Maclaurin spheroids in the limit of vanishing viscosity [1–3]. In meteorology this phenomenon is known as the 'Holopäinen instability mechanism' for a baroclinic flow when waves that are linearly stable in the absence of Ekman friction become dissipatively destabilized in its presence, with the result that the location of the curve of marginal stability is displaced by an order one distance in the parameter space, even if the Ekman number is infinitesimally small [5,12–15]. A similar effect in solid mechanics is represented by the 'Ziegler destabilization paradox' [7,16–19].

Swaters noticed in [13] that the stability boundary associated with the zero dissipation limit of a dissipative baroclinic instability theory does not collapse to the inviscid result when the Ekman dissipation is replaced by other dissipative mechanisms, e.g. by horizontal turbulent friction, confirming that such a *singular limit* is generic. However, he also managed to choose a specific dissipative perturbation (in which the dissipation is proportional to the geostrophic potential vorticity) possessing coincidence of the zero dissipation limit of the dissipative marginal stability boundary with the inviscid result [13].

The destabilization by dissipation is especially intriguing when several diffusion mechanisms act simultaneously [2,20–24]. In this case, 'no simple rule for the effect of introducing small viscosity or diffusivity on flows that are neutral in their absence appears to hold' [25]. In hydrodynamics, a classical example is given by secular instability of the Maclaurin spheroids due to both fluid viscosity and gravitational radiation reaction, where the critical eccentricity of the meridional section of the spheroid depends on the *ratio* of the two dissipative mechanisms and reaches its maximum, corresponding to the onset of dynamical instability in the ideal system, exactly when this ratio equals 1 [2,22]. In solid mechanics, the generic character of the discontinuity of the instability threshold in the zero dissipation limit was already noticed in the work by Smith [26,27], who found that a viscoelastic shaft rotating in bearings with viscous damping is prone to dissipation-induced instability for almost all ratios of the damping coefficient of the shaft and the damping coefficient of the bearings, except one specific ratio.

In hydrodynamics and magnetohydrodynamics (MHD) the ratio of damping coefficients corresponding to different dissipative mechanisms is traditionally called *the Prandtl number*. For example, the Prandtl number, $Pr = \nu/\kappa$, measures the relative strength of the diffusion of vorticity represented in the Navier–Stokes equations by the kinematic viscosity coefficient ν and thermal diffusion with the coefficient of thermal diffusivity κ [28,29]. The magnetic Prandtl number, $Pm = \nu/\eta$, is the ratio of the coefficients of the kinematic viscosity and ohmic diffusion, η [28–30]. To get an idea of the key role of the Prandtl numbers in the correspondence between stability criteria in the diffusionless and the double-diffusive case, let us consider the Rayleigh centrifugal instability criterion and its extensions.

Downloaded from http://rspa.royalsocietypublishing.org/ on September 13, 2017

The Rayleigh criterion [30] predicts a stationary axisymmetric instability of an ideal incompressible Newtonian fluid, differentially rotating with the radially varying angular velocity $\Omega = \Omega(r)$ if

$$Ro + 1 < 0, \tag{1.1}$$

where Ro is the fluid Rossby number

$$Ro := \frac{r\partial_r \Omega}{2\Omega} \tag{1.2}$$

and $\partial_r = \partial/\partial r$. For a viscous fluid, the Rayleigh criterion (1.1) is modified as follows [34]:

$$Ro + 1 + \frac{1}{4Re^2} < 0 \tag{1.3}$$

and reduces to the diffusionless criterion (1.1) as the Reynolds number, $Re \to \infty$.

In the general multiple-diffusive case, the existence of such a direct correspondence between the diffusionless and diffusive stability criteria is not evident. In many cases, however, the reduction of the double-diffusive instability criteria to the diffusionless ones can be achieved by setting the corresponding Prandtl number to a specific value, e.g. to 1, and then tending diffusivities to zero (or, equivalently, the corresponding Reynolds numbers to infinity) [22].

For example, the stationary axisymmetric instability known as the double-diffusive Goldreich–Schubert–Fricke (GSF) instability [28,29,35] develops in a rotating viscous and thermally conducting fluid when the extended Rayleigh criterion is fulfilled [28]:

$$4(Ro + 1) + Pr\frac{N^2}{\Omega^2} + \frac{1}{Re^2} < 0, \tag{1.4}$$

where N is the Brunt–Väisälä frequency[1] [36],

$$N^2 := \frac{g}{\gamma}\frac{\partial}{\partial r}\ln(p\rho^{-\gamma}) = \frac{g}{\gamma}\left(\frac{1}{p}\frac{\partial p}{\partial r} - \frac{\gamma}{\rho}\frac{\partial \rho}{\partial r}\right),$$

and p is the pressure of the fluid, ρ the density, γ the adiabatic index and g the radial acceleration. When dissipative effects are absent, $\nu = 0$, $\kappa = 0$, the diffusionless GSF instability occurs for [28]

$$4(Ro + 1) + \frac{N^2}{\Omega^2} < 0. \tag{1.5}$$

Evidently, $Pr = 1$ is the only value at which the criterion (1.4) reduces to (1.5) in the limit $Re \to \infty$.

Similarly, Michael's criterion of ideal MHD [37] predicts stationary axisymmetric instability caused by an azimuthal magnetic field for a rotating flow of a non-viscous incompressible Newtonian fluid that is a perfect electrical conductor if [37]

$$Ro + 1 - \frac{\omega_{A_\phi}^2}{\Omega^2} Rb < 0, \tag{1.6}$$

where Rb is the magnetic Rossby number [38],

$$Rb := \frac{r\partial_r \omega_{A_\phi}}{2\omega_{A_\phi}}, \tag{1.7}$$

and ω_{A_ϕ} is the Alfvén angular velocity related to the magnitude of the magnetic field [39]. Again, the diffusionless Michael's criterion (1.6) follows in the limit of $Re \to \infty$ from its double-diffusive

[1]Which in the limit of $\gamma \to \infty$ reduces to the buoyancy frequency in the Boussinesq approximation $N^2 = -(g/\rho)(\mathrm{d}\rho/\mathrm{d}r)$.

Downloaded from http://rspa.royalsocietypublishing.org/ on September 13, 2017

counterpart[2] [28,43]

$$Ro + 1 - Pm\frac{\omega_{A_\phi}^2}{\Omega^2}Rb + \frac{1}{4\,Re^2} < 0 \tag{1.8}$$

only if $Pm = 1$.

In particular, Michael's criterion for both the diffusionless and the double-diffusive problem predicts stability with respect to axisymmetric perturbations for the rotating flow and the azimuthal magnetic field that satisfy the following constraints:

$$\Omega = \omega_{A_\phi} \quad \text{and} \quad Ro = Rb = -1. \tag{1.9}$$

In 1956, Chandrasekhar [44] observed that the properties (1.9) correspond to an exact steady solution of the MHD equations for an incompressible fluid in the ideal case, i.e. when $\nu = 0$ and $\eta = 0$. For this solution, the total pressure of the fluid and the magnetic field are constant, the fluid velocity at every point is parallel to the direction of the magnetic field at that point and the Alfvén angular velocity is equal to the angular velocity of the fluid, which implies equality of the densities of the fluid magnetic and kinetic energies. This *energy equipartition solution* of the ideal MHD was proved by Chandrasekhar [44] to be marginally stable against *general* perturbations.[3]

To illustrate stability of the equipartition solution (1.9) with respect to non-axisymmetric perturbations, we substitute it into the following criterion of destabilization of a hydrodynamically stable rotating flow of an inviscid and perfectly conducting fluid by an azimuthal magnetic field:

$$\frac{\omega_{A_\phi}^2}{\Omega^2} < -\frac{4Ro}{m^2}, \tag{1.10}$$

where $m \gg 1$ is the azimuthal wavenumber and $Ro < 0$ [28,39,47]. The criterion (1.10) is valid in the limit of infinitely large axial and azimuthal wavenumbers of the perturbation. Naturally, the solution (1.9) violates (1.10) already at $m \geq 2$, thus confirming the Chandrasekhar theorem [44].

Recently, Bogoyavlenskij [48] discovered that viscous and resistive incompressible MHD equations possess exact *unsteady* equipartition solutions with finite and equal kinetic and magnetic energies when the fluid velocity and the magnetic field are collinear and the kinematic viscosity ν is equal to the magnetic diffusivity η, i.e. when $Pm = 1$. Under the constraint $Pm = 1$, the Bogoyavlenskij unsteady equipartition solutions turn into the ideal and *steady* Chandrasekhar equipartition equilibria when $\nu = \eta \to 0$ [48].

One could expect, that in double-diffusive MHD, the remarkable stability of the Chandrasekhar energy equipartition solution is preserved under the constraint $Pm = 1$. As soon as the constraint is violated, one could anticipate a dissipation-induced instability of the equipartition solution. For instance, recent analytical works [38,43] demonstrated that, in the inductionless limit[4] of $Pm = 0$, a rotating viscous incompressible fluid with vanishing electrical

[2]By analysing the criterion (1.8) for the case of the rigid-body rotation ($Ro = 0$), Acheson & Hide [40] came to the conclusion that the electrical resistance of the fluid opposes the destabilizing influence of a radial increase of the magnetic field (when $Rb > 0$) and that viscous effects support it. They supposed that 'the damping effect of viscosity on the disturbances is offset by its action as an agent for diffusion of momentum, which reduces the stabilizing effect of rigid-body rotation by enabling the circulation of a displaced ring of fluid to harmonize more readily with its surroundings'. These ideas were further developed in [28,41,42] with application to double-diffusive convection in a stratified fluid.

[3]A bit surprisingly, as he admitted in his memoirs [45]: 'One nice result which nevertheless came out at this time was the proof of the stability of the equipartition solution. Wentzel and Goldberger checked my analysis as I could not quite believe the result myself'. Actually, the Chandrasekhar equipartition solution belongs to a wide class of exact stationary solutions of MHD equations for the case of ideal incompressible infinitely conducting fluid with constant total pressure that includes even flows with knotted magnetic surfaces [46].

[4]A very small ratio of viscosity of the fluid to its electrical resistivity, typically of order 10^{-6}–10^{-5}, is a characteristic of liquid metals that are used in laboratory experiments, e.g. with the magnetized Couette–Taylor flow [49] and von Karman flow [50]. Recently developed Newtonian magnetic liquid metal suspensions have a tunable Pm in the diapason from 10^{-6} to 10^{-4} [51]. In astrophysics and geophysics such small values of Pm are typical for the planetary interiors, cold parts of accretion discs, and 'dead-zones' of the protoplanetary discs [28–30,36,38,43,52–54].

Downloaded from http://rspa.royalsocietypublishing.org/ on September 13, 2017

conductivity is destabilized by azimuthal magnetic fields of arbitrary radial dependency if

$$8(Ro+1)\,Rb > -(Ro+2)^2. \tag{1.11}$$

The above inequality predicts the onset of the azimuthal magnetorotational instability (AMRI) even in the case of the Keplerian rotating flow with $Ro = -\frac{3}{4}$ when $Rb > -25/32$ [38]. In particular, (1.11) implies destabilization of the Chandrasekhar equipartition solution, whose susceptibility to the double-diffusive AMRI at $Pm \ll 1$ has been confirmed numerically in [53,54].

According to the group-theoretical argument by Julien & Knobloch [55], AMRI is an oscillatory instability with a non-zero azimuthal wavenumber, which is most likely to develop in the presence of the azimuthal magnetic field [49,56]. Hence, its onset in the double-diffusion case is characterized by the classical Hopf bifurcation, at which simple eigenvalues cross the imaginary axis in the complex plane. On the other hand, the equations of the diffusionless MHD can be written in Hamiltonian form [57]. For this reason, the stable oscillatory non-axisymmetric modes in the ideal MHD case can carry both positive and negative energy; their interaction yields the Hamilton–Hopf bifurcation at the onset of the non-axisymmetric oscillatory instabilities [58].

In this study, we perform a local stability analysis of a circular Couette–Taylor flow of a viscous and electrically conducting fluid in an azimuthal magnetic field of arbitrary radial dependence. We obtain a unifying geometric picture that naturally connects the diffusionless and double-diffusive AMRI in low- and high-Pm regimes in the spirit of the singularity theory approach by Bottema [17], Arnold [59] and Langford [11] on generic singularities in the multiparameter families of matrices, which is especially efficient when combined with the perturbation of multiple eigenvalues, index theory and exploitation of the fundamental symmetries of the ideal system [6,8,60–62].

After a brief re-derivation of the already known equations of the system in the short-wavelength approximation, we write the corresponding algebraic eigenvalue problem, which determines the dispersion relation, as a non-Hamiltonian perturbation of a Hamiltonian eigenvalue problem. The latter yields the dispersion relation of the ideal system. This allows us to investigate systematically the singular limit of the onset of the oscillatory AMRI due to the classical Hopf bifurcation at arbitrary Pm when viscous and resistive terms tend to zero.

In the frame of the local stability analysis, we show that the threshold of the double-diffusive AMRI tends to the threshold of the diffusionless AMRI only at $Pm = 1$ as the Reynolds numbers tend to infinity and find the Whitney umbrella singularity on the neutral stability surface that dictates this specific choice of Pm. We classify the stable oscillatory modes involved in the Hamilton–Hopf bifurcation by their Krein (or energy) sign. Then, we explicitly demonstrate by means of the perturbation theory for eigenvalues that when viscosity and ohmic diffusivity are weak (and even infinitesimally small), the dominance of viscosity destroys the stability of the negative energy mode at $Pm > 1$, whereas the dominance of ohmic diffusivity destabilizes the positive energy mode at $Pm < 1$ (including the inductionless case $Pm = 0$) in the close vicinity of the Hamilton–Hopf bifurcation. However, when the fluid Rossby number exceeds some critical value, the destabilization is possible only at finite values of Reynolds numbers and is accompanied by a transfer of instability between negative- and positive-energy modes that occurs due to the presence of complex exceptional points in the spectrum. This clarifies the reasons for instability of Chandrasekhar's equipartition solution and its extensions at both low and high Pm.

2. Transport equation for amplitudes and its dispersion relation

(a) Governing equations and the background fields

The dynamics of a flow of a viscous and electrically conducting incompressible fluid that interacts with the magnetic field is described by the Navier–Stokes equation for fluid velocity $\boldsymbol{u}$ which is

Downloaded from http://rspa.royalsocietypublishing.org/ on September 13, 2017

coupled with the induction equation for magnetic field $\boldsymbol{B}$ [36,43]:

$$\left.\begin{aligned}&\frac{\partial \boldsymbol{u}}{\partial t}+\boldsymbol{u}\cdot\boldsymbol{\nabla}\boldsymbol{u}-\frac{1}{\mu_0\rho}\boldsymbol{B}\cdot\boldsymbol{\nabla}\boldsymbol{B}+\frac{1}{\rho}\boldsymbol{\nabla}P-\nu\boldsymbol{\nabla}^2\boldsymbol{u}=0\\ \text{and}\quad&\frac{\partial \boldsymbol{B}}{\partial t}+\boldsymbol{u}\cdot\boldsymbol{\nabla}\boldsymbol{B}-\boldsymbol{B}\cdot\boldsymbol{\nabla}\boldsymbol{u}-\eta\boldsymbol{\nabla}^2\boldsymbol{B}=0.\end{aligned}\right\}\tag{2.1}$$

In equations (2.1), the total pressure is defined by $P=p+\boldsymbol{B}^2/2\mu_0$, where p is the hydrodynamic pressure, $\rho=$ const. the density, $\nu=$ const. the kinematic viscosity, $\eta=(\mu_0\sigma)^{-1}$ the magnetic diffusivity, $\sigma=$ const. the conductivity of the fluid and μ_0 is the magnetic permeability of free space. In addition, the incompressible flow and the solenoidal magnetic field fulfil the constraints

$$\boldsymbol{\nabla}\cdot\boldsymbol{u}=0\quad\text{and}\quad\boldsymbol{\nabla}\cdot\boldsymbol{B}=0.\tag{2.2}$$

It is well known that, for a flow differentially rotating in a gap between the radii r_1 and $r_2>r_1$, equations (2.1) and (2.2) possess a steady solution of the general form [53,63]

$$\boldsymbol{u}_0(r)=r\,\Omega(r)\,\boldsymbol{e}_\phi,\quad p=p_0(r)\quad\text{and}\quad\boldsymbol{B}_0(r)=B_\phi^0(r)\boldsymbol{e}_\phi\tag{2.3}$$

in the cylindrical coordinate system (r,ϕ,z). In the *magnetized circular Couette–Taylor flow* (2.3), the angular velocity profile $\Omega(r)$ and the azimuthal magnetic field $B_\phi^0(r)$ are arbitrary functions of the radial coordinate r satisfying boundary conditions for an inviscid and non-resistive fluid [53,63]. For a viscous and resistive fluid, the angular velocity has the form $\Omega(r)=a+br^{-2}$, while the expression for the magnetic field is given by $B_\phi^0(r)=cr+dr^{-1}$ with the coefficients determined from boundary conditions [53,63]. In the frame of the local linear stability analysis of the flow (2.3) that will be performed in the following, boundary conditions are ignored and the steady state of the double diffusive system is also the steady state of the diffusionless system.

In 1956, Chandrasekhar [44] observed that for the exact stationary solution (2.3) of equations (2.1) and (2.2) with $\Omega=B_\phi^0/(r\sqrt{\rho\mu_0})$ and $P=$ const. in the ideal case, i.e. when $\nu=0$ and $\eta=0$, the kinetic and magnetic energies are in equipartition, $\rho(\Omega r)^2/2=(B_\phi^0)^2/(2\mu_0)$, and $Ro=Rb=-1$. The latter equality follows from the condition of constant total pressure and from the fact that, in the steady state, the centrifugal acceleration of the background flow is compensated by the pressure gradient, $r\Omega^2=(1/\rho)\partial_r p_0$ [43]. Note that $Ro=-1$ corresponds to the velocity profile $\Omega(r)\sim r^{-2}$, whereas $Rb=-1$ corresponds to the magnetic field produced by an axial current I isolated from the fluid [43,49,53]: $B_\phi^0(r)=\mu_0 I/(2\pi r)$.

Linearizing equations (2.1) and (2.2) in the vicinity of the stationary solution (2.3) by assuming general perturbations $\boldsymbol{u}=\boldsymbol{u}_0+\boldsymbol{u}'$, $p=p_0+p'$ and $\boldsymbol{B}=\boldsymbol{B}_0+\boldsymbol{B}'$, leaving only the terms of first order with respect to the primed quantities, and introducing the gradients of the background fields represented by the two 3×3 matrices

$$\mathcal{U}:=\boldsymbol{\nabla}\boldsymbol{u}_0=\Omega\begin{pmatrix}0&-1&0\\1+2Ro&0&0\\0&0&0\end{pmatrix}\quad\text{and}\quad\mathcal{B}:=\boldsymbol{\nabla}\boldsymbol{B}_0=\frac{B_\phi^0}{r}\begin{pmatrix}0&-1&0\\1+2Rb&0&0\\0&0&0\end{pmatrix},\tag{2.4}$$

we arrive at the linearized system of MHD [38,43,64]

$$\begin{pmatrix}\partial_t+\mathcal{U}+\boldsymbol{u}_0\cdot\boldsymbol{\nabla}-\nu\boldsymbol{\nabla}^2&-\dfrac{\mathcal{B}+\boldsymbol{B}_0\cdot\boldsymbol{\nabla}}{\rho\mu_0}\\ \mathcal{B}-\boldsymbol{B}_0\cdot\boldsymbol{\nabla}&\partial_t-\mathcal{U}+\boldsymbol{u}_0\cdot\boldsymbol{\nabla}-\eta\boldsymbol{\nabla}^2\end{pmatrix}\begin{pmatrix}\boldsymbol{u}'\\\boldsymbol{B}'\end{pmatrix}=-\frac{\boldsymbol{\nabla}}{\rho}\begin{pmatrix}p'+\dfrac{\boldsymbol{B}_0\cdot\boldsymbol{B}'}{\mu_0}\\0\end{pmatrix},\tag{2.5}$$

where the perturbations fulfil the constraints

$$\boldsymbol{\nabla}\cdot\boldsymbol{u}'=0,\quad\boldsymbol{\nabla}\cdot\boldsymbol{B}'=0.\tag{2.6}$$

Downloaded from http://rspa.royalsocietypublishing.org/ on September 13, 2017

(b) Derivation of the amplitude transport equations

Let ϵ be a small parameter ($0 < \epsilon \ll 1$). We seek solutions of the linearized equations (2.5) in the form of asymptotic expansions with respect to the small parameter ϵ [65]:

$$\boldsymbol{L}'(\boldsymbol{x},t,\epsilon) = \mathrm{e}^{\mathrm{i}\Phi(\boldsymbol{x},t)/\epsilon}(\boldsymbol{L}^{(0)}(\boldsymbol{x},t) + \epsilon \boldsymbol{L}^{(1)}(\boldsymbol{x},t,)) + \epsilon \boldsymbol{L}^{(r)}(\boldsymbol{x},t,\epsilon), \tag{2.7}$$

where $\boldsymbol{L}' = (\boldsymbol{u}', \boldsymbol{B}', p')^{\mathrm{T}}$, $\boldsymbol{L}^{(j)} = (\boldsymbol{u}^{(j)}, \boldsymbol{B}^{(j)}, p^{(j)})^{\mathrm{T}}$, $\boldsymbol{x}$ is a vector of coordinates, Φ represents the phase of the wave or the eikonal, and $\boldsymbol{u}^{(j)}$, $\boldsymbol{B}^{(j)}$ and $p^{(j)}$, $j = 0, 1, r$, are complex-valued amplitudes. The index r denotes the remainder terms that are assumed to be uniformly bounded in ϵ on any fixed time interval [66,67].

Maslov [68] observed that high-frequency oscillations $\exp(\mathrm{i}\epsilon^{-1}\Phi(\boldsymbol{x},t))$ quickly die out because of viscosity unless one assumes a quadratic dependency of viscosity on the small parameter ϵ. Following [34,68,69], we assume that $\nu = \epsilon^2\tilde{\nu}$ and $\eta = \epsilon^2\tilde{\eta}$.

Substituting expansions (2.7) in (2.5) and collecting terms at ϵ^{-1} and ϵ^0, we find [43]

$$\epsilon^{-1}: \begin{pmatrix} \partial_t\Phi + (\boldsymbol{u}_0\cdot\boldsymbol{\nabla}\Phi) & -\dfrac{(\boldsymbol{B}_0\cdot\boldsymbol{\nabla}\Phi)}{\rho\mu_0} \\ -(\boldsymbol{B}_0\cdot\boldsymbol{\nabla}\Phi) & \partial_t\Phi + (\boldsymbol{u}_0\cdot\boldsymbol{\nabla}\Phi) \end{pmatrix} \begin{pmatrix} \boldsymbol{u}^{(0)} \\ \boldsymbol{B}^{(0)} \end{pmatrix} = -\frac{\boldsymbol{\nabla}\Phi}{\rho} \begin{pmatrix} p^{(0)} + \dfrac{\boldsymbol{B}_0\cdot\boldsymbol{B}^{(0)}}{\mu_0} \\ 0 \end{pmatrix} \tag{2.8}$$

and

$$\begin{aligned} \epsilon^0: \mathrm{i} &\begin{pmatrix} \partial_t\Phi + (\boldsymbol{u}_0\cdot\boldsymbol{\nabla}\Phi) & -\dfrac{(\boldsymbol{B}_0\cdot\boldsymbol{\nabla}\Phi)}{\rho\mu_0} \\ -(\boldsymbol{B}_0\cdot\boldsymbol{\nabla}\Phi) & \partial_t\Phi + (\boldsymbol{u}_0\cdot\boldsymbol{\nabla}\Phi) \end{pmatrix} \begin{pmatrix} \boldsymbol{u}^{(1)} \\ \boldsymbol{B}^{(1)} \end{pmatrix} + \mathrm{i}\frac{\boldsymbol{\nabla}\Phi}{\rho} \begin{pmatrix} p^{(1)} + \dfrac{\boldsymbol{B}_0\cdot\boldsymbol{B}^{(1)}}{\mu_0} \\ 0 \end{pmatrix} \\ &+ \begin{pmatrix} \partial_t + \mathcal{U} + \boldsymbol{u}_0\cdot\boldsymbol{\nabla} + \tilde{\nu}(\boldsymbol{\nabla}\Phi)^2 & -\dfrac{\mathcal{B} + \boldsymbol{B}_0\cdot\boldsymbol{\nabla}}{\rho\mu_0} \\ \mathcal{B} - \boldsymbol{B}_0\cdot\boldsymbol{\nabla} & \partial_t - \mathcal{U} + \boldsymbol{u}_0\cdot\boldsymbol{\nabla} + \tilde{\eta}(\boldsymbol{\nabla}\Phi)^2 \end{pmatrix} \begin{pmatrix} \boldsymbol{u}^{(0)} \\ \boldsymbol{B}^{(0)} \end{pmatrix} \\ &+ \frac{\boldsymbol{\nabla}}{\rho} \begin{pmatrix} p^{(0)} + \dfrac{\boldsymbol{B}_0\cdot\boldsymbol{B}^{(0)}}{\mu_0} \\ 0 \end{pmatrix} = 0. \end{aligned} \tag{2.9}$$

The solenoidality conditions (2.6) yield

$$\left.\begin{aligned} \boldsymbol{u}^{(0)}\cdot\boldsymbol{\nabla}\Phi = 0, \quad \boldsymbol{\nabla}\cdot\boldsymbol{u}^{(0)} + \mathrm{i}\boldsymbol{u}^{(1)}\cdot\boldsymbol{\nabla}\Phi = 0 \\ \text{and} \qquad \boldsymbol{B}^{(0)}\cdot\boldsymbol{\nabla}\Phi = 0, \quad \boldsymbol{\nabla}\cdot\boldsymbol{B}^{(0)} + \mathrm{i}\boldsymbol{B}^{(1)}\cdot\boldsymbol{\nabla}\Phi = 0. \end{aligned}\right\} \tag{2.10}$$

Taking the dot product of the first of the equations in system (2.8) with $\boldsymbol{\nabla}\Phi$ under the constraints (2.10), we find that, for $\boldsymbol{\nabla}\Phi \neq 0$,

$$p^{(0)} = -\frac{\boldsymbol{B}_0\cdot\boldsymbol{B}^{(0)}}{\mu_0}. \tag{2.11}$$

Under condition (2.11), equation (2.8) has a non-trivial solution if the determinant of the 6×6 matrix in its left-hand side vanishes. This gives us two characteristic roots corresponding to the two Alfvén waves [64,65] that yield the following two Hamilton–Jacobi equations:

$$\partial_t\Phi + \left(\boldsymbol{u}_0 \pm \frac{\boldsymbol{B}_0}{\sqrt{\rho\mu_0}}\right)\cdot\boldsymbol{\nabla}\Phi = 0. \tag{2.12}$$

The characteristic roots $\left(-\boldsymbol{u}_0 \pm \boldsymbol{B}_0/\sqrt{\rho\mu_0}\right)\cdot\boldsymbol{\nabla}\Phi$ are triple and semi-simple and degenerate into a semi-simple characteristic root of multiplicity 6 on the surface [64,65]

$$\boldsymbol{B}_0\cdot\boldsymbol{\nabla}\Phi = 0. \tag{2.13}$$

When (2.13) is fulfilled, the derivative of the phase along the fluid stream lines vanishes:

$$\frac{\mathrm{D}\Phi}{\mathrm{D}t} := \partial_t\Phi + \boldsymbol{u}_0\cdot\boldsymbol{\nabla}\Phi = 0. \tag{2.14}$$

Downloaded from http://rspa.royalsocietypublishing.org/ on September 13, 2017

Using relations (2.11), (2.13) and (2.14), we simplify equations (2.9):

$$\left.\begin{aligned}&\left(\frac{\mathrm{D}}{\mathrm{D}t}+\tilde{\nu}(\boldsymbol{\nabla}\Phi)^2+\mathcal{U}\right)\boldsymbol{u}^{(0)}-\frac{1}{\rho\mu_0}(\mathcal{B}+\boldsymbol{B}_0\cdot\boldsymbol{\nabla})\boldsymbol{B}^{(0)}=-\frac{\mathrm{i}}{\rho}\left(p^{(1)}+\frac{1}{\mu_0}(\boldsymbol{B}_0\cdot\boldsymbol{B}^{(1)})\right)\boldsymbol{\nabla}\Phi\\ \text{and}\quad&\left(\frac{\mathrm{D}}{\mathrm{D}t}+\tilde{\eta}(\boldsymbol{\nabla}\Phi)^2-\mathcal{U}\right)\boldsymbol{B}^{(0)}+(\mathcal{B}-\boldsymbol{B}_0\cdot\boldsymbol{\nabla})\boldsymbol{u}^{(0)}=0.\end{aligned}\right\}\tag{2.15}$$

Eliminating pressure in the first of equations (2.15) via multiplication of it by $\boldsymbol{\nabla}\Phi$ and taking into account the constraints (2.10), then using the identities

$$\left.\begin{aligned}\boldsymbol{\nabla}\partial_t\Phi+\boldsymbol{\nabla}(\boldsymbol{u}_0\cdot\boldsymbol{\nabla})\Phi&=\frac{\mathrm{D}}{\mathrm{D}t}\boldsymbol{\nabla}\Phi+\mathcal{U}^{\mathrm{T}}\boldsymbol{\nabla}\Phi=0,\\ \boldsymbol{\nabla}(\boldsymbol{B}_0\cdot\boldsymbol{\nabla}\Phi)&=(\boldsymbol{B}_0\cdot\boldsymbol{\nabla})\boldsymbol{\nabla}\Phi+\mathcal{B}^{\mathrm{T}}\boldsymbol{\nabla}\Phi=0,\\ \frac{\mathrm{D}}{\mathrm{D}t}(\boldsymbol{\nabla}\Phi\cdot\boldsymbol{u}^{(0)})&=\frac{\mathrm{D}\boldsymbol{\nabla}\Phi}{\mathrm{D}t}\cdot\boldsymbol{u}^{(0)}+\boldsymbol{\nabla}\Phi\cdot\frac{D\boldsymbol{u}^{(0)}}{\mathrm{D}t}=0\\ \text{and}\qquad(\boldsymbol{B}_0\cdot\boldsymbol{\nabla})(\boldsymbol{\nabla}\Phi\cdot\boldsymbol{B}^{(0)})&=((\boldsymbol{B}_0\cdot\boldsymbol{\nabla})\boldsymbol{\nabla}\Phi)\cdot\boldsymbol{B}^{(0)}+\boldsymbol{\nabla}\Phi\cdot(\boldsymbol{B}_0\cdot\boldsymbol{\nabla})\boldsymbol{B}^{(0)}=0,\end{aligned}\right\}\tag{2.16}$$

and, finally, defining $\boldsymbol{k}=\boldsymbol{\nabla}\Phi$, we write the transport equations for the amplitudes (2.15) as

$$\left.\begin{aligned}\frac{\mathrm{D}\boldsymbol{u}^{(0)}}{\mathrm{D}t}&=-\left(\mathcal{I}-\frac{2\boldsymbol{k}\boldsymbol{k}^{\mathrm{T}}}{|\boldsymbol{k}|^2}\right)\mathcal{U}\boldsymbol{u}^{(0)}-\tilde{\nu}|\boldsymbol{k}|^2\boldsymbol{u}^{(0)}+\frac{1}{\rho\mu_0}\left(\left(\mathcal{I}-\frac{2\boldsymbol{k}\boldsymbol{k}^{\mathrm{T}}}{|\boldsymbol{k}|^2}\right)\mathcal{B}+\boldsymbol{B}_0\cdot\boldsymbol{\nabla}\right)\boldsymbol{B}^{(0)}\\ \text{and}\quad\frac{\mathrm{D}\boldsymbol{B}^{(0)}}{\mathrm{D}t}&=\mathcal{U}\boldsymbol{B}^{(0)}-\tilde{\eta}|\boldsymbol{k}|^2\boldsymbol{B}^{(0)}-(\mathcal{B}-\boldsymbol{B}_0\cdot\boldsymbol{\nabla})\boldsymbol{u}^{(0)},\end{aligned}\right\}\tag{2.17}$$

where $\mathcal{I}$ is the 3×3 identity matrix. From phase equation (2.16), we deduce that

$$\frac{\mathrm{D}\boldsymbol{k}}{\mathrm{D}t}=-\mathcal{U}^{\mathrm{T}}\boldsymbol{k}.\tag{2.18}$$

Equations (2.17) and (2.18) are valid under the assumption that condition (2.13) is fulfilled.

Local partial differential equations (2.17) are fully equivalent to the transport equations of [8,43]. In the case of the ideal MHD when viscosity and resistivity are zero, equations (2.17) exactly coincide with those of the work [64] and are fully equivalent to the transport equations derived in [70]. In the absence of the magnetic field, these equations are reduced to that of the work [34] that considered stability of the viscous Couette–Taylor flow.

Note that the leading-order terms dominate solution (2.7) for a sufficiently long time, provided that ϵ is small enough [66,67], which reduces analysis of instabilities to the investigation of the growth rates of solutions of transport equations (2.17).

According to [34,70], in order to study physically relevant and potentially unstable modes, we have to choose bounded and asymptotically non-decaying solutions of system (2.18). These correspond to $k_\phi\equiv0$, and k_R and k_z time-independent. Note that this solution is compatible with the constraint $\boldsymbol{B}_0\cdot\boldsymbol{k}=0$ following from (2.13).

(c) Dispersion relation of the double-diffusive amplitude equations

Define $\alpha=k_z|\boldsymbol{k}|^{-1}$, $|\boldsymbol{k}|^2=k_R^2+k_z^2$ and introduce the Alfvén angular velocity, the viscous and resistive frequencies, and the hydrodynamic and magnetic Reynolds numbers [43]:

$$\omega_{A_\phi}=\frac{B_\phi^0}{R\sqrt{\rho\mu_0}},\quad\omega_\nu=\tilde{\nu}|\boldsymbol{k}|^2,\quad\omega_\eta=\tilde{\eta}|\boldsymbol{k}|^2,\quad Re=\frac{\alpha\Omega}{\omega_\nu}\quad\text{and}\quad Rm=\frac{\alpha\Omega}{\omega_\eta}.\tag{2.19}$$

In particular, $Rm=Re\,Pm$.

Downloaded from http://rspa.royalsocietypublishing.org/ on September 13, 2017

Looking for a solution to equations (2.17) in the modal form [70]: $\boldsymbol{u}^{(0)} = \hat{\boldsymbol{u}}\,\mathrm{e}^{\alpha\Omega\lambda t+\mathrm{i}m\phi}$, $\boldsymbol{B}^{(0)} = \sqrt{\rho\mu_0}\hat{\boldsymbol{B}}\,\mathrm{e}^{\alpha\Omega\lambda t+\mathrm{i}m\phi}$, we write the amplitude equations in the matrix form

$$\mathbf{A}\mathbf{z} = \lambda\mathbf{z}, \tag{2.20}$$

where $\mathbf{z} = (\hat{u}_R, \hat{u}_\phi, \hat{B}_R, \hat{B}_\phi)^{\mathrm{T}} \in \mathbb{C}^4$ and $\mathbf{A} = \mathbf{A}_0 + \mathbf{A}_1 \in \mathbb{C}^{4\times4}$ with [38,43,71]

$$\mathbf{A}_0 = \begin{pmatrix} -\mathrm{i}n & 2\alpha & \mathrm{i}nS & -2\alpha S \\ -\dfrac{2(1+Ro)}{\alpha} & -\mathrm{i}n & \dfrac{2(1+Rb)}{\alpha}S & \mathrm{i}nS \\ \mathrm{i}nS & 0 & -\mathrm{i}n & 0 \\ -\dfrac{2Rb}{\alpha}S & \mathrm{i}nS & \dfrac{2Ro}{\alpha} & -\mathrm{i}n \end{pmatrix}, \quad \mathbf{A}_1 = \begin{pmatrix} \dfrac{-1}{Re} & 0 & 0 & 0 \\ 0 & \dfrac{-1}{Re} & 0 & 0 \\ 0 & 0 & \dfrac{-1}{Rm} & 0 \\ 0 & 0 & 0 & \dfrac{-1}{Rm} \end{pmatrix}. \tag{2.21}$$

The ratio $n = m/\alpha$ is the modified azimuthal wavenumber and $S = \omega_{A_\phi}/\Omega$ is the Alfvén angular velocity in the units of Ω.

Let us introduce a Hermitian matrix

$$\mathbf{G} = \begin{pmatrix} 0 & -\mathrm{i} & 0 & \mathrm{i}S \\ \mathrm{i} & 0 & -\mathrm{i}S & 0 \\ 0 & \mathrm{i}S & 4\dfrac{Ro-Rb}{\alpha n} & -\mathrm{i} \\ -\mathrm{i}S & 0 & \mathrm{i} & 0 \end{pmatrix} \tag{2.22}$$

and define an indefinite inner product in $\mathbb{C}^4$ as $[\mathbf{x},\mathbf{y}] = \bar{\mathbf{y}}^{\mathrm{T}}\mathbf{G}\mathbf{x}$ [8,72] and a standard inner product as $(\mathbf{x},\mathbf{y}) = \bar{\mathbf{y}}^{\mathrm{T}}\mathbf{x}$. The matrix $\mathbf{H}_0 = -\mathrm{i}\mathbf{G}\mathbf{A}_0$ is Hermitian too:

$$\mathbf{H}_0 = \begin{pmatrix} -\dfrac{2(S^2Rb-Ro-1)}{\alpha} & \mathrm{i}n(S^2+1) & -\dfrac{2S(1+Rb-Ro)}{\alpha} & -2\mathrm{i}nS \\ -\mathrm{i}n(S^2+1) & 2\alpha & 2\mathrm{i}nS & -2\alpha S \\ -\dfrac{2S(1+Rb-Ro)}{\alpha} & -2\mathrm{i}nS & \dfrac{2(S^2Rb+S^2+2Rb-3Ro)}{\alpha} & \mathrm{i}n(S^2+1) \\ 2\mathrm{i}nS & -2\alpha S & -\mathrm{i}n(S^2+1) & 2\alpha S^2 \end{pmatrix}. \tag{2.23}$$

Consequently, the eigenvalue problem $\mathbf{A}_0\mathbf{z} = \lambda\mathbf{z}$ can be written in the Hamiltonian form with the Hamiltonian $\mathbf{H}_0$ [8,72,73]:

$$\mathbf{H}_0\mathbf{z} = \mathrm{i}^{-1}\mathbf{G}\lambda\mathbf{z}. \tag{2.24}$$

The fundamental symmetry

$$\mathbf{A}_0 = -\mathbf{G}^{-1}\overline{\mathbf{A}_0}^{\mathrm{T}}\mathbf{G}, \tag{2.25}$$

where the overbar denotes complex conjugation, implies the symmetry of the spectrum of the matrix $\mathbf{A}_0$ with respect to the imaginary axis [8,72].

The full eigenvalue problem (2.20) is thus a dissipative perturbation of the Hamiltonian eigenvalue problem (2.24):

$$(\mathbf{H}_0 + \mathbf{H}_1)\mathbf{z} = \mathrm{i}^{-1}\mathbf{G}\lambda\mathbf{z}, \tag{2.26}$$

where $\mathbf{H}_1 = -\mathrm{i}\mathbf{G}\mathbf{A}_1$ is a complex non-Hermitian matrix:

$$\mathbf{H}_1 = \begin{pmatrix} 0 & \dfrac{1}{Re} & 0 & -\dfrac{S}{Rm} \\ -\dfrac{1}{Re} & 0 & \dfrac{S}{Rm} & 0 \\ 0 & -\dfrac{S}{Re} & 4\mathrm{i}\dfrac{Ro-Rb}{\alpha nRm} & \dfrac{1}{Rm} \\ \dfrac{S}{Re} & 0 & -\dfrac{1}{Rm} & 0 \end{pmatrix}. \tag{2.27}$$

Downloaded from http://rspa.royalsocietypublishing.org/ on September 13, 2017

The complex characteristic equation $p(\lambda) := \det(\mathbf{H}_0 + \mathbf{H}_1 - \mathrm{i}^{-1}\mathbf{G}\lambda\mathbf{I}) = 0$, where $\mathbf{I}$ is the 4×4 identity matrix, is the dispersion relation for the double-diffusive system (2.26).

3. Linear Hamilton–Hopf bifurcation and the diffusionless AMRI

(a) Krein sign and splitting of double eigenvalues with Jordan block

Consider the unperturbed (Hamiltonian) case corresponding to $\mathbf{H}_1 = 0$. A simple imaginary eigenvalue $\lambda = \mathrm{i}\omega$ of the eigenvalue problem (2.24) with the eigenvector $\mathbf{z}$ is said to have positive Krein sign if $[\mathbf{z}, \mathbf{z}] > 0$ and negative Krein sign if $[\mathbf{z}, \mathbf{z}] < 0$ [8,72].

Denote by $\mathbf{p}$ the vector of all parameters of the matrix $\mathbf{H}_0$: $\mathbf{p} = (S, Ro, Rb, n)^{\mathrm{T}} \in \mathbb{R}^4$. Let at $\mathbf{p} = \mathbf{p}_0$ the matrix $\mathbf{H}_0 = \mathbf{H}(\mathbf{p}_0)$ have a double imaginary eigenvalue $\lambda = \mathrm{i}\omega_0$ ($\omega_0 \geq 0$) with the Jordan chain consisting of the eigenvector $\mathbf{z}_0$ and the associated vector $\mathbf{z}_1$ that satisfy the following equations [8,72]:

$$\mathbf{H}_0\mathbf{z}_0 = \omega_0\mathbf{G}\mathbf{z}_0 \quad \text{and} \quad \mathbf{H}_0\mathbf{z}_1 = \omega_0\mathbf{G}\mathbf{z}_1 + \mathrm{i}^{-1}\mathbf{G}\mathbf{z}_0. \tag{3.1}$$

Transposing these equations and applying the complex conjugation yields

$$\bar{\mathbf{z}}_0^{\mathrm{T}}\mathbf{H}_0 = \omega_0\bar{\mathbf{z}}_0^{\mathrm{T}}\mathbf{G} \quad \text{and} \quad \bar{\mathbf{z}}_1^{\mathrm{T}}\mathbf{H}_0 = \omega_0\bar{\mathbf{z}}_1^{\mathrm{T}}\mathbf{G} - \mathrm{i}^{-1}\bar{\mathbf{z}}_0^{\mathrm{T}}\mathbf{G}. \tag{3.2}$$

As a consequence, $\bar{\mathbf{z}}_0^{\mathrm{T}}\mathbf{G}\mathbf{z}_0 = 0$ and $\bar{\mathbf{z}}_1^{\mathrm{T}}\mathbf{G}\mathbf{z}_0 + \bar{\mathbf{z}}_0^{\mathrm{T}}\mathbf{G}\mathbf{z}_1 = 0$ or, in the other notation,

$$[\mathbf{z}_0, \mathbf{z}_0] = 0 \quad \text{and} \quad [\mathbf{z}_0, \mathbf{z}_1] = -[\mathbf{z}_1, \mathbf{z}_0]. \tag{3.3}$$

Varying parameters along a curve $\mathbf{p} = \mathbf{p}(\varepsilon)$ ($\mathbf{p}(0) = \mathbf{p}_0$), where ε is a real parameter, and assuming the Newton–Puiseux expansions for the double eigenvalue $\mathrm{i}\omega_0$ and its eigenvector in powers of $\varepsilon^{1/2}$ when $|\varepsilon|$ is small, we find [8]

$$\lambda_\pm = \mathrm{i}\omega_0 \pm \mathrm{i}\omega_1\varepsilon^{1/2} + o(\varepsilon^{1/2}) \quad \text{and} \quad \mathbf{z}_\pm = \mathbf{z}_0 \pm \mathrm{i}\omega_1\mathbf{z}_1\varepsilon^{1/2} + o(\varepsilon^{1/2}), \tag{3.4}$$

with

$$\omega_1 = \sqrt{\mathrm{i}\frac{\bar{\mathbf{z}}_0^{\mathrm{T}}\Delta\mathbf{H}\mathbf{z}_0}{\bar{\mathbf{z}}_1^{\mathrm{T}}\mathbf{G}\mathbf{z}_0}} \quad \text{and} \quad \Delta\mathbf{H} = \sum_{s=1}^{4}\frac{\partial\mathbf{H}}{\partial p_s}\frac{\mathrm{d}p_s}{\mathrm{d}\varepsilon}\bigg|_{\varepsilon=0} = \overline{(\Delta\mathbf{H})}^{\mathrm{T}}. \tag{3.5}$$

Taking into account that $\bar{\mathbf{z}}_0^{\mathrm{T}}\Delta\mathbf{H}\mathbf{z}_0$ is real and $\bar{\mathbf{z}}_1^{\mathrm{T}}\mathbf{G}\mathbf{z}_0$ is imaginary, we assume that $\omega_1 > 0$, which is a reasonable assumption in view of the fact that $\omega_0 > 0$ and $|\varepsilon|$ is small. Then, for $\varepsilon > 0$, the double eigenvalue $\mathrm{i}\omega_0$ splits into two pure imaginary ones $\lambda_\pm = \mathrm{i}\omega_0 \pm \mathrm{i}\omega_1\sqrt{\varepsilon}$ (stability). When $\varepsilon < 0$, the splitting yields a pair of complex eigenvalues with real parts of different sign (instability). Therefore, varying parameters along a curve $\mathbf{p}(\varepsilon)$, we have a linear Hamilton–Hopf bifurcation at the point $\mathbf{p}_0$, which is a regular point of the boundary between the domains of stability and oscillatory instability. The path $\mathbf{p}(\varepsilon)$ crosses the stability boundary at the point $\mathbf{p}_0$.

Calculating the indefinite inner product for the perturbed eigenvectors $\mathbf{z}_\pm$ at $\varepsilon > 0$, we find [8]

$$[\mathbf{z}_+, \mathbf{z}_+] = +2\mathrm{i}\omega_1\bar{\mathbf{z}}_0^{\mathrm{T}}\mathbf{G}\mathbf{z}_1\varepsilon^{1/2} + o(\varepsilon^{1/2}) \quad \text{and} \quad [\mathbf{z}_-, \mathbf{z}_-] = -2\mathrm{i}\omega_1\bar{\mathbf{z}}_0^{\mathrm{T}}\mathbf{G}\mathbf{z}_1\varepsilon^{1/2} + o(\varepsilon^{1/2}). \tag{3.6}$$

Therefore, the simple imaginary eigenvalue λ_+ with the eigenvector $\mathbf{u}_+$ has the Krein sign which is opposite to the Krein sign of the eigenvalue λ_- with the eigenvector $\mathbf{u}_-$. With decreasing $\varepsilon > 0$, the imaginary eigenvalues λ_+ and λ_- with opposite Krein signs move towards each other along the imaginary axis until at $\varepsilon = 0$ (i.e. at $\mathbf{p} = \mathbf{p}_0$) they merge and form the double imaginary eigenvalue $\mathrm{i}\omega_0$, which further splits into two complex eigenvalues when ε takes negative values. The opposite Krein signs is a necessary and sufficient condition for the imaginary eigenvalues participating in the merging to leave the imaginary axis [6,72,73]. Below we demonstrate the Krein collision at the onset of the diffusionless AMRI by calculating the roots of the dispersion relation both analytically and numerically.

Downloaded from http://rspa.royalsocietypublishing.org/ on September 13, 2017

(b) Neutral stability curves

Let $\delta := Ro - RbS^2$. In the Hamiltonian case ($1/Re = 0$, $1/Rm = 0$), the dispersion relation $p_0(\lambda) := \det(\mathbf{H}_0 - i^{-1}\mathbf{G}\lambda\mathbf{I}) = 0$ possesses a compact representation [39,43,70]

$$p_0(\lambda) = 4\delta^2 + 4(\mathrm{i}\lambda - n + nS^2)^2 - \left(2\delta - (\mathrm{i}\lambda - n)^2 + n^2S^2\right)^2 = 0. \tag{3.7}$$

If $\delta = 0$, i.e. $Ro = RbS^2$, then equation (3.7) simplifies and its roots are [43]

$$\left.\begin{aligned} \lambda_{1,2} &= -\mathrm{i}(1+n) \pm \mathrm{i}\sqrt{1 - S^2[1-(1+n)^2]} \\ \text{and} \quad \lambda_{3,4} &= -\mathrm{i}(1-n) \pm \mathrm{i}\sqrt{1 - S^2[1-(1-n)^2]}. \end{aligned}\right\} \tag{3.8}$$

The eigenvalues $\lambda_{1,2,3,4}$ are imaginary and simple for all $0 < n \leq 2$ if $0 \leq S < 1$. The equality $S = 1$ implies $Ro = Rb$ and the existence of a double zero eigenvalue which is semi-simple at all $0 \leq n \leq 2$ except $n = 1$ where it has a Jordan block of order 2; the other two eigenvalue branches are formed by simple imaginary eigenvalues (marginal stability). At $S > 1$, complex eigenvalues originate (oscillatory instability) if

$$S > \frac{1}{\sqrt{1-(1-n)^2}}. \tag{3.9}$$

At the boundary of domain (3.9), the eigenvalues are double imaginary with a Jordan block.

In general, the instability corresponds to the negative discriminant of polynomial (3.7):

$$\begin{aligned} &(nS)^6(S^2-1)^2 + 2(nS)^4[(S^2+1)\delta^2 + 2(S^2-1)(S^2-2)\delta + (S^2-1)^2(1-2S^2)] \\ &\quad + (nS)^2[\delta^4 + 4(2S^2+3)\delta^3 - 2(4S^4 + 11(S^2-1))\delta^2 + 4(S^2-1)(5S^2-3)\delta + (S^2-1)^2] \\ &\quad - 4\delta(\delta+1)^3(S^2-\delta-1) < 0. \end{aligned} \tag{3.10}$$

Following [39], we assume in (3.10) that $nS = c$, where $c = \mathrm{const}$. Taking into account that $\delta = Ro - RbS^2$ and then taking the limit $S \to 0$, which obviously corresponds to the limit of $n \to \infty$, we find the following asymptotic expression for the instability condition [39]:

$$(c^2 + 4Ro)((Ro+1)^2 + c^2)^2 < 0,$$

or $S^2 < -4Ro/n^2$, which yields (1.10) at $\alpha = 1$. At $n = 0$, inequality (3.10) reduces to $\delta < -1$, which is exactly the diffusionless Michael criterion (1.6).

Let us now assume that $S = 1$. Then, inequality (3.10) takes the form

$$4n^4 + ((Ro-Rb)^2 + 20(Ro-Rb) - 8)n^2 + 4(Ro - Rb + 1)^3 < 0 \tag{3.11}$$

and the dispersion relation at $S = 1$ factorizes as follows:

$$p_0(\lambda)|_{S=1} = [\lambda^3 + 4in\lambda^2 + 4(1 - n^2 + Ro - Rb)\lambda + 8in(Ro - Rb)]\lambda = 0. \tag{3.12}$$

The equality in (3.11) corresponds to the transition from marginal stability to oscillatory instability via the linear Hamilton–Hopf bifurcation (figure 1). At the marginal stability curve with $S = 1$, one of the eigenvalues λ is always zero and simple, another one is simple and imaginary, and the last two form a double and imaginary eigenvalue with the Jordan block. At $S = 1$ and $Rb = -1$, the critical value of the fluid Rossby number follows from (3.11) and is equal to

$$Ro_c(n) = -2 + \frac{\beta^{1/3} - n^2}{12} - \frac{n^2}{\beta^{1/3}}\left(18 - \frac{n^2}{12}\right), \tag{3.13}$$

where

$$\beta(n) = -n^2\left(n^4 + 540n^2 - 5832 - 24\sqrt{3(n^2+27)^3}\right). \tag{3.14}$$

Downloaded from http://rspa.royalsocietypublishing.org/ on September 13, 2017

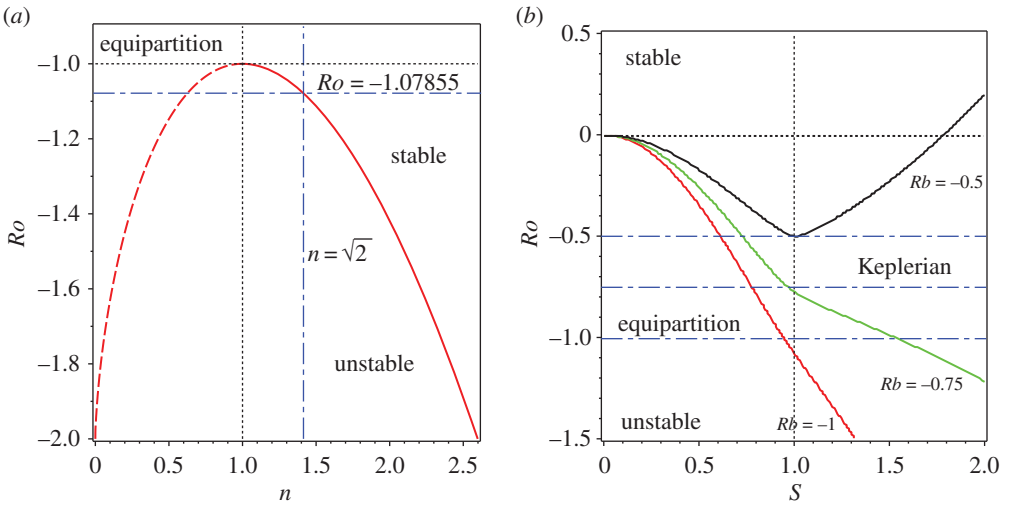

Figure 1. (*a*) Stability diagram in (n, Ro)-plane at $S = 1$ and $Rb = -1$ according to the criterion (3.11). The dashed line shows the non-physical branch of the neutral stability curve (3.13) corresponding to $0 < n < 1$. (*b*) The critical value of Ro at the onset of the Hamilton–Hopf bifurcation as a function of S when $n = \sqrt{-2Rb}$ [43] at various values of Rb. (Online version in colour.)

For example, at $n = \sqrt{2}$ equation (3.13) yields $Ro_c \approx -1.07855$, corresponding to the intersection of the two dash-dot lines in figure 1*a*. At this point of the curve (3.13) the eigenvalues are $\lambda_1 = \lambda_2 = \lambda_c$ (figure 2), where

$$\left.\begin{aligned} \lambda_c = \frac{i\sqrt{2}}{34347}\left\{\frac{9\sqrt{87}+136}{4}[\beta(\sqrt{2})]^{2/3} + \frac{321\sqrt{87}-2782}{2}[\beta(\sqrt{2})]^{1/3} - 57245\right\} \approx -i0.43046 \\ \text{and} \quad \lambda_3 \approx -i4.79594, \quad \lambda_4 = 0. \end{aligned}\right\} \tag{3.15}$$

Naturally, such explicit expressions for double imaginary eigenvalues can be obtained with the use of (3.13) and (3.14) for any other value of n. The choice of n does not influence the qualitative picture of eigenvalue interaction shown in figure 2. The value $n = \sqrt{2}$ is known to be optimal in several respects [43,56,74], which will be discussed further in the text.

(c) The Krein collision at the linear Hamilton–Hopf bifurcation threshold

Although it is easy to evaluate the Krein sign of the imaginary eigenvalues shown in figure 1 numerically, it is instructive first to do it analytically in a particular case when $Ro = Rb = -1$ and $S = 1$. Then, the eigenvalues are given explicitly by equation (3.8), which yields a double semi-simple zero eigenvalue $\lambda_0 = 0$ with two linearly independent eigenvectors $\mathbf{z}_1 = (0, 1, 0, 1)^T$ and $\mathbf{z}_2 = (1, 0, 1, 0)^T$ and two imaginary eigenvalues $\lambda_\pm = -2i(n \pm 1)$ with eigenvectors $\mathbf{z}_+ = (-i\alpha, -n/(2+n), i n\alpha/(2+n), 1)^T$ and $\mathbf{z}_- = (i\alpha, n/(2-n), i n\alpha/(2-n), 1)^T$, respectively (figure 2*a*).

Notice that the eigenvalues λ_+ and λ_- of Chandrasekhar's equipartition solution have the opposite Krein signs:

$$\frac{[\mathbf{z}_+, \mathbf{z}_+]}{(\mathbf{z}_+, \mathbf{z}_+)} = -\frac{2\alpha}{1+\alpha^2}\frac{2(n+1)^2}{1+(n+1)^2} < 0 \quad \text{and} \quad \frac{[\mathbf{z}_-, \mathbf{z}_-]}{(\mathbf{z}_-, \mathbf{z}_-)} = \frac{2\alpha}{1+\alpha^2}\frac{2(n-1)^2}{1+(n-1)^2} > 0. \tag{3.16}$$

For instance, at $n = \sqrt{2}$ we have $((1+\alpha^2)/2\alpha)([\mathbf{z}_-, \mathbf{z}_-]/(\mathbf{z}_-, \mathbf{z}_-)) = 1 - \sqrt{2}/2 \approx 0.2929$, which implies that λ_- has a positive Krein sign (figure 3*a*). The solid circle corresponding to λ_- in figure 3*a* belongs to the curve of the values of the normalized indefinite inner products $[\mathbf{z}, \mathbf{z}]/(\mathbf{z}, \mathbf{z})$ calculated on the eigenvectors at the eigenvalues of the branch marked as λ_2 in figure 2*a*. All imaginary eigenvalues λ_2 for $Ro_c < Ro < -1$ have positive Krein sign. By contrast, the eigenvalues of the branch λ_1 in figure 2*a* have negative Krein sign on the same interval.

Downloaded from http://rspa.royalsocietypublishing.org/ on September 13, 2017

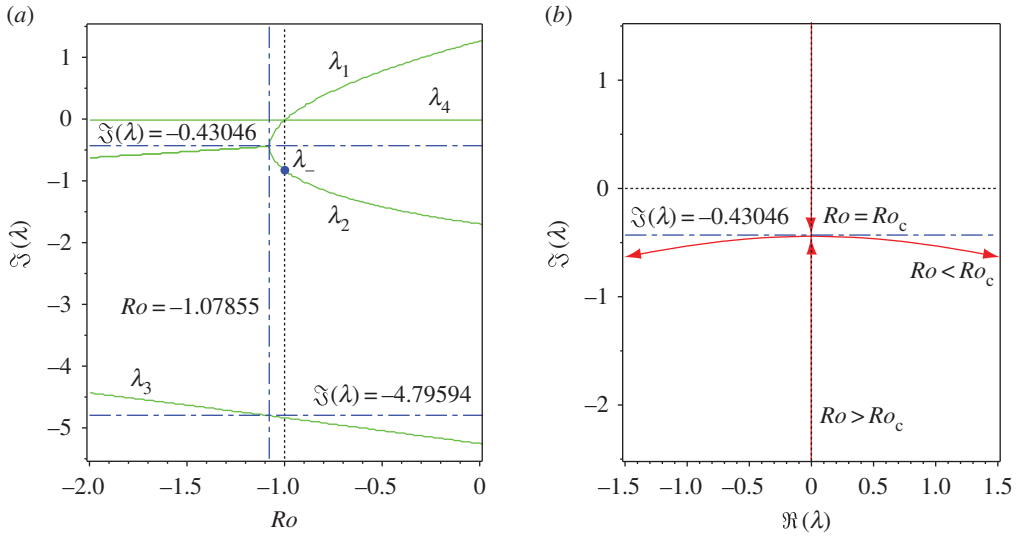

Figure 2. (*a*) Typical evolution of frequencies of the roots of the dispersion relation (3.12) as *Ro* is varied, shown for $S = 1$, $Rb = -1$ and $n = \sqrt{2}$ that correspond to crossing the neutral stability curve along the vertical dash-dot line in figure 1*a*. It demonstrates the Hamilton–Hopf bifurcation at $Ro = Ro_c \approx -1.07855$ and the marginal stability of the Chandrasekhar energy equipartition solution at $Ro = -1$. (*b*) The same linear Hamilton–Hopf bifurcation shown in the complex plane: with the decrease in *Ro*, two simple imaginary eigenvalues collide into a double imaginary eigenvalue with the Jordan block (an *exceptional point* [8]) that subsequently splits into two complex eigenvalues (oscillatory instability). (Online version in colour.)

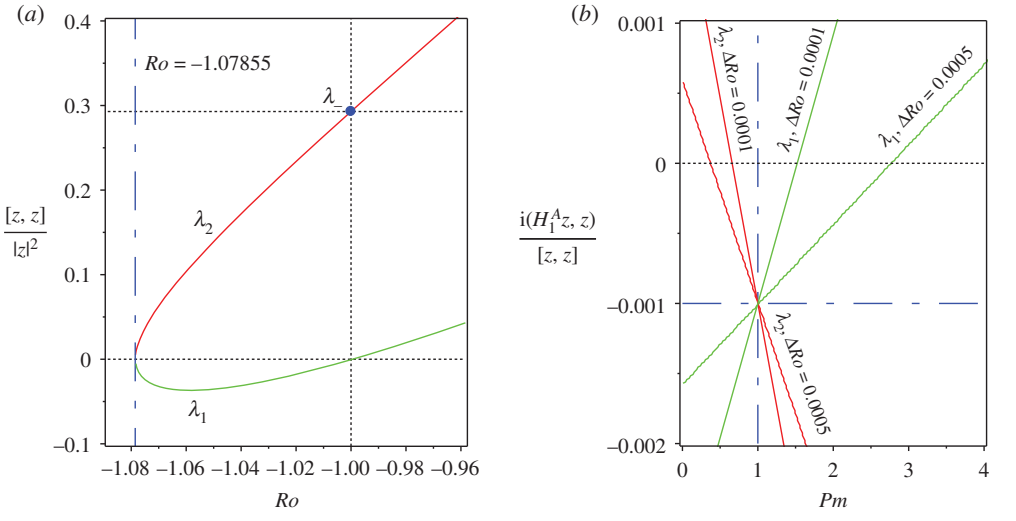

Figure 3. For $S = 1$, $Rb = -1$, $n = \sqrt{2}$ and $\alpha = 1$ (*a*) the values of the normalized indefinite inner product $[\mathbf{z}, \mathbf{z}]/(\mathbf{z}, \mathbf{z})$ calculated with the eigenvectors at the imaginary eigenvalues λ_1 and λ_2 shown in figure 2*a* that participate in the Hamilton–Hopf bifurcation at $Ro = Ro_c \approx -1.07855$. For $Ro_c < Ro < -1$, the Krein sign of λ_1 is negative and the Krein sign of λ_2 is positive. (*b*) For $Rm = 1000$, the values of the real increment $\delta\lambda^A$ to eigenvalues λ_1 with the negative Krein sign and to eigenvalues λ_2 with the positive Krein sign according to equation (4.1). The interval of negative increments (stability) around $Pm = 1$ becomes narrower as $\Delta Ro := Ro - Ro_c$ tends to zero. (Online version in colour.)

Therefore, the onset of the non-axisymmetric oscillatory instability (or the diffusionless AMRI) is accompanied by the Krein collision of modes of positive and negative Krein sign, in accordance with the results of the §3a. The Krein sign is directly related to the sign of energy of a mode and

Downloaded from http://rspa.royalsocietypublishing.org/ on September 13, 2017

the linear Hamilton–Hopf bifurcation is a collision of two imaginary eigenvalues of a Hamiltonian system with the opposite Krein (energy) signs [6,8,58,72,73].

4. Dissipation-induced instabilities of the double-diffusive system

(a) Dissipative perturbation of simple imaginary eigenvalues

The complex non-Hermitian matrix of the dissipative perturbation can be decomposed into its Hermitian and anti-Hermitian components: $\mathbf{H}_1 = \mathbf{H}_1^{\mathrm{H}} + \mathbf{H}_1^{\mathrm{A}}$, where

$$\mathbf{H}_1^{\mathrm{H}} = \frac{S(Pm-1)}{2Rm}\begin{pmatrix} 0 & 0 & 0 & 1 \\ 0 & 0 & -1 & 0 \\ 0 & -1 & 0 & 0 \\ 1 & 0 & 0 & 0 \end{pmatrix}$$

and

$$\mathbf{H}_1^{\mathrm{A}} = \frac{1}{Rm}\begin{pmatrix} 0 & Pm & 0 & -\dfrac{S(Pm+1)}{2} \\ -Pm & 0 & \dfrac{S(Pm+1)}{2} & 0 \\ 0 & -\dfrac{S(Pm+1)}{2} & 4\mathrm{i}\dfrac{Ro-Rb}{\alpha n} & 1 \\ \dfrac{S(Pm+1)}{2} & 0 & -1 & 0 \end{pmatrix}.$$

At large Rm, an increment $\delta\lambda$ to a simple imaginary eigenvalue λ with an eigenvector $\mathbf{z}$ is given by a standard perturbation theory [4,8,60,61] as

$$\delta\lambda = \mathrm{i}\frac{\bar{\mathbf{z}}^{\mathrm{T}}\mathbf{H}_1\mathbf{z}}{\bar{\mathbf{z}}^{\mathrm{T}}\mathbf{G}\mathbf{z}} = \mathrm{i}\frac{(\mathbf{H}_1\mathbf{z},\mathbf{z})}{[\mathbf{z},\mathbf{z}]}. \tag{4.1}$$

The increment $\delta\lambda^{\mathrm{H}} = \mathrm{i}((\mathbf{H}_1^{\mathrm{H}}\mathbf{z},\mathbf{z})/[\mathbf{z},\mathbf{z}])$ is obviously imaginary. In particular, $\mathbf{H}_1^{\mathrm{H}} = 0$ at $Pm = 1$, i.e. the frequencies are not affected by the Hermitian component of the dissipative perturbation if the contributions from viscosity and resistivity are equal.

By contrast, the increment $\delta\lambda^{\mathrm{A}} = \mathrm{i}((\mathbf{H}_1^{\mathrm{A}}\mathbf{z},\mathbf{z})/[\mathbf{z},\mathbf{z}])$ is real. For instance, the eigenvalues λ_+ and λ_- of Chandrasekhar's equipartition solution acquire the following increments:

$$\delta\lambda_{\pm}^{\mathrm{A}} = -\frac{Pm+1}{2Rm} = -\frac{1}{h} := -\frac{1}{2}\left(\frac{1}{Re}+\frac{1}{Rm}\right), \quad \delta\lambda_{\pm}^{\mathrm{H}} = 0, \tag{4.2}$$

where h is the harmonic mean of the two Reynolds numbers.

(b) Weak ohmic diffusion destabilizes positive energy waves at low *Pm*

In the close vicinity of the critical Rossby number of the Hamilton–Hopf bifurcation $Ro_{\mathrm{c}} \approx -1.07855$, the real increment $\delta\lambda^{\mathrm{A}}$ to imaginary eigenvalues λ_1 with negative Krein sign and λ_2 with positive Krein sign are shown in figure 3*b* for fixed $Rm = 10^3$ and varying Pm (the fluid Reynolds number is calculated as $Re = Rm/Pm$).

The eigenvalues with the *negative* Krein sign become dissipatively destabilized when $Pm > 1$, i.e. when the losses due to viscosity of the fluid exceed the ohmic losses (cf. [40]). Remarkably, the eigenvalues with the *positive* Krein sign can also acquire positive growth rates. However, this happens at $Pm < 1$ when the electrical resistivity prevails over the kinematic viscosity. Indeed, the destabilizing influence of the kinematic viscosity of the fluid on negative energy waves is well known in hydrodynamics [6,20,25,40], which therefore places the dissipation-induced instability at $Pm > 1$ and $|Ro - Ro_{\mathrm{c}}| \ll 1$ into an established context. The destabilization of positive energy modes was noticed in the context of solid mechanics, in particular, in gyroscopic systems with damping and non-conservative positional (or circulatory, or curl [75]) forces in [7,8,27,62].

Downloaded from http://rspa.royalsocietypublishing.org/ on September 13, 2017

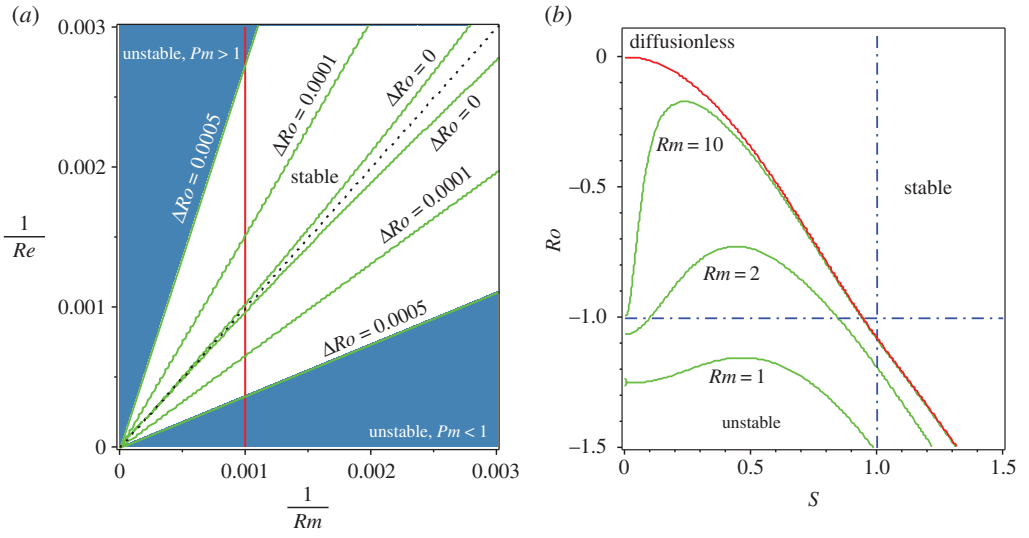

Figure 4. (*a*) For $S = 1$, $Rb = -1$ and $n = \sqrt{2}$, the neutral stability curves in the plane (Rm^{-1}, Re^{-1}) of the inverse magnetic and fluid Reynolds numbers corresponding to different values of $\Delta Ro := Ro - Ro_c$. The stability domain has a shape of an angular sector at $\Delta Ro > 0$ and a cusp at $\Delta Ro = 0$ with the single tangent line $Pm = 1$ (cf. figure 3*b*). (*b*) The neutral stability curves for $Rb = -1$, $n = \sqrt{2}$ and $Re = Rm$ in the (S, Ro)-plane at various values of Rm. (Online version in colour.)

Radiative dissipation due to emission of electromagnetic, acoustic and gravitational waves is a well-known reason for instability of modes of positive energy in hydrodynamics and plasma physics [2,22,23,76]. To the best of our knowledge, the dissipative destabilization of the positive energy modes due to ohmic losses has not been previously reported in MHD.

The interval of negative real increments in figure 3*b* decreases with the decrease in deviation from the critical value of the Rossby number at the Hamilton–Hopf bifurcation, i.e. as $\Delta Ro = Ro - Ro_c$ tends to zero. When $\Delta Ro = 0$, the stable interval reduces to the single value: $Pm = 1$. Hence, weak ohmic diffusion (weak kinematic viscosity) destabilizes positive (negative) energy waves at $Pm < 1$ ($Pm > 1$) if $|Ro - Ro_c|$ is sufficiently small.

(c) Diffusionless and double-diffusive criteria are connected at $Pm = 1$

We complement the sensitivity analysis of eigenvalues of the diffusionless Hamiltonian eigenvalue problem with respect to a double-diffusive perturbation with the direct computation of the stability boundaries based on the algebraic Bilharz stability criterion. The Bilharz criterion [77] guarantees localization of all the roots of a complex polynomial of degree n to the left of the imaginary axis in the complex plane, provided that all principal minors of even order of the $2n \times 2n$ Bilharz matrix composed of the real and imaginary parts of the coefficients of the polynomial are positive [8].

Applying the Bilharz criterion to the characteristic polynomial of the eigenvalue problem (2.26), we plot the neutral stability curves in the plane of the inverse Reynolds numbers Rm^{-1} and Re^{-1} at various values of $\Delta Ro = Ro - Ro_c$, where Ro_c is defined in (3.13), when $S = 1$, $Rb = -1$ and $n = \sqrt{2}$ (figure 4*a*). Note that the diagonal ray corresponding to $Pm = 1$ always stays in the stability domain when $\Delta Ro \geq 0$ and is the only tangent line to the stability boundary at the cuspidal point at the origin when $Ro = Ro_c$. Moreover, at $Ro = Ro_c$ and $Re = Rm$ the spectrum of the double-diffusive system with $S = 1$ and $Rb = -1$ contains the double complex eigenvalues (exceptional points [8])

$$\lambda_d = \lambda_c(n) - Rm^{-1}. \tag{4.3}$$

The imaginary eigenvalue $\lambda_c(n)$ is given in (3.15) for the particular case of $n = \sqrt{2}$.

Downloaded from http://rspa.royalsocietypublishing.org/ on September 13, 2017

Approaching the origin along the ray $Pm = 1$ means letting the Reynolds numbers tend to infinity with their ratio being kept equal to unity. Figure 4*b* demonstrates that, in the limit $Re = Rm \to \infty$, the neutral stability curve of the double-diffusive system approaches the threshold of instability of the diffusionless system from below. The instability domain of the double-diffusive system always remains smaller than in the diffusionless case. As a consequence, the Chandrasekhar equipartition solution ($Ro = Rb = -1, S = 1$), being stable in the diffusionless case, remains stable at $Pm = 1$ no matter what the value of the Reynolds numbers is (figure 4*b*).

Indeed, in the case when $Ro = RbS^2$ and $Re = Rm$, the roots of the characteristic polynomial of the eigenvalue problem (2.26) can be found explicitly

$$\left.\begin{aligned}\lambda_{1,2} &= -\mathrm{i}(n+1) - \frac{1}{Rm} \pm \mathrm{i}\sqrt{1 - S^2[1-(n+1)^2]}\\ \text{and}\qquad \lambda_{3,4} &= -\mathrm{i}(n-1) - \frac{1}{Rm} \pm \mathrm{i}\sqrt{1 - S^2[1-(n-1)^2]}.\end{aligned}\right\} \tag{4.4}$$

The eigenvalues (4.4) are just the eigenvalues (3.8) that are shifted by dissipation to the left in the complex plane (asymptotic stability). This fact agrees perfectly with the result of Bogoyavlenskij [48], who found at $Pm = 1$ exact unsteady energy equipartition solutions of the viscous and resistive incompressible MHD equations that relax with the growth rate equal to $-1/Re = -1/Rm < 0$ to the ideal and steady Chandrasekhar equipartition equilibria [44]. Note also that even earlier Lerner and Knobloch reported a 'cooperative, accelerated decay' of solutions at $Pm = 1$ in the study of stability of the magnetized plane Couette flow [33].

Well known is a similar result on the secular instability of the Maclaurin spheroids due to both fluid viscosity and gravitational radiation reaction[5] when the value of the critical eccentricity of the meridional section at the onset of instability in the ideal case is attained only when the ratio of the two dissipation mechanisms is exactly 1 [22,76].

(d) Double-diffusive instability at $Pm \neq 1$ and arbitrary *Re* and *Rm*

(i) Unfolding the Hamilton–Hopf bifurcation in the vicinity of $Pm = 1$

Along $Re = Rm > 0$ the variation of Ro at fixed $Rb = -1$, $S = 1$, and n is accompanied by a bifurcation at $Ro = Ro_c$ of the double complex eigenvalue (4.3) with negative real part equal to $-Rm^{-1}$ (figure 5*a*). Effectively, at $Pm = 1$ dissipation shifts the Hamilton–Hopf bifurcation to the left in the complex plane. For this reason, the oscillatory instability in the double-diffusive system with equal viscosity and resistivity occurs through the classical Hopf bifurcation at $Ro(Rm) < Ro_c$ with $Ro(Rm)$ tending to Ro_c as $Rm \to \infty$.

In the case when the magnetic Prandtl number slightly deviates from the value $Pm = 1$, the shifted Hamilton–Hopf bifurcation unfolds into a couple of quasi-hyperbolic eigenvalue branches passing close to each other in an avoided crossing centred at an exceptional point λ_d of the family (4.3) with real part equal to $-h^{-1}$, where $h = 2/(1/Re + 1/Rm)$ is the harmonic mean of the fluid and magnetic Reynolds numbers, $Re \neq Rm$ (figure 5*a*).

The unfolding of the eigenvalue crossing into the avoided crossing can happen in two different ways depending on the sign of $Pm - 1$. At $Pm < 1$ ($Pm > 1$), the complex eigenvalues stemming from the imaginary eigenvalues of the diffusionless system with positive (negative) Krein sign form a branch that bends to the right and crosses the imaginary axis at some $Ro(Re, Rm) \neq Ro_c$ (figure 5*a*, cf. [2]). The critical values $Ro(Re, Rm)$ of the double-diffusive system live on the surface in the (Re^{-1}, Rm^{-1}, Ro)-space that has a self-intersection along the Ro-axis (figure 5*b*). The angle of the self-intersection tends to zero as $Ro \to Ro_c$ and at the point $(0, 0, Ro_c)$ the surface has a singularity known as the Whitney umbrella[6] [7,11,59].

[5]The dissipation-induced instability of Maclaurin spheroids due to emission of gravitational waves is known as the Chandrasekhar–Friedman–Schutz (CFS) instability [76].

[6]The normal form of a surface in the $Oxyz$-space that has the Whitney umbrella singular point at the origin is given by the equation $zy^2 = x^2$ [11,17,59].

Downloaded from http://rspa.royalsocietypublishing.org/ on September 13, 2017

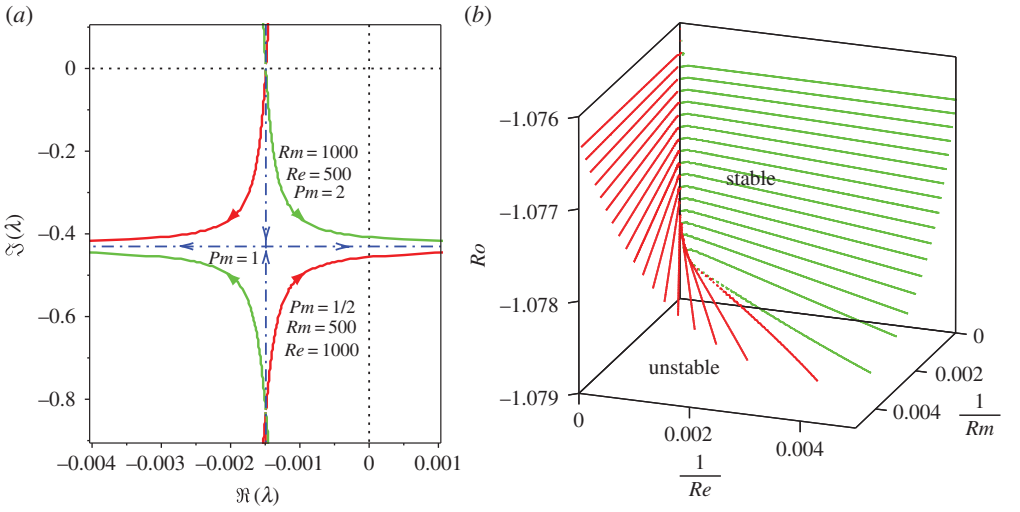

Figure 5. (*a*) At $Rb = -1$, $S = 1$ and $n = \sqrt{2}$, the dash-dot lines show interaction of complex eigenvalues with negative real parts in the complex λ-plane with the decrease in Ro when $Re = Rm = h = 2/(1/500 + 1/1000)$, i.e. $Pm = 1$. At $Ro = Ro_c$, the eigenvalues merge into the double complex eigenvalue (4.3). The quasi-hyperbolic curves demonstrate the imperfect merging of modes (the avoided crossing) such that the mode with positive Krein (energy) sign becomes unstable at $Pm < 1$ and the mode with negative Krein (energy) sign is unstable at $Pm > 1$. (*b*) The neutral stability surface represented by the contours $Ro = \text{const.}$ in the (Re^{-1}, Rm^{-1}, Ro)-space has a 'Whitney umbrella' singular point at $(0, 0, Ro_c)$ yielding a cusp in the cross section $Ro = Ro_c$ with the single tangent line $Pm = 1$. (Online version in colour.)

In the vicinity of the Ro-axis, the instability threshold is effectively a ruled surface [17], where the slope of each ruler is determined by Pm. Letting the Reynolds numbers tend to infinity while keeping the magnetic Prandtl number fixed means that the Ro-axis is approached in the (Re^{-1}, Rm^{-1}, Ro)-space along a ruler corresponding to this value of Pm. Generically, for all values of Pm except $Pm = 1$, a ruler leads to a limiting value of Ro that exceeds Ro_c and thus extends the instability interval of the fluid Rossby numbers with respect to that of the diffusionless system, as is visible in figures 5*b* and 6*a*. The plane $Pm = 1$ divides the neutral stability surface in the vicinity of $Ro = Ro_c$ into two parts corresponding to positive energy modes destabilized by the dominating ohmic diffusion at $Pm < 1$ and to negative energy modes destabilized by the dominating fluid viscosity at $Pm > 1$ (figure 5*b*). The ray determined by the conditions $Re = Rm > 0$, $Ro = Ro_c$ belongs to the stability domain of the double-diffusive system and contains exceptional points (4.3) that determine[7] behaviour of eigenvalues shown in figure 5*a*.

Figure 6*a* shows that, at a fixed $Pm \neq 1$, the critical value of Ro at the onset of the double-diffusive AMRI is displaced by an order one distance along the Ro-axis with respect to the critical value Ro_c of the diffusionless case, when both viscous and ohmic diffusion tend to zero. This effect does not depend on the choice of n (figure 6*b*). Indeed, the critical values of Ro in the limit of vanishing dissipation at a fixed Pm and $S = 1$ and $Rb = -1$ satisfy the following equation:

$$(Pm+1)^3 n^2 (3Ro^2 - 4n^2 - 14Ro - 9) + 4(PmRo - 3Ro - 4)(2PmRo + 3Pm + 1)^2 = 16(Pm+1)Pm(Ro+1)^2 n^2. \tag{4.5}$$

Using this equation, one can easily check analytically that the critical Ro has its minimum at $Pm = 1$, independent of the choice of n (figure 6*c*, cf. [22]). Nevertheless, the displacement is rather small if $Pm \in [0, 1]$, with the maximum attained at $Pm = 0$ where the diffusionless limit

[7]This was anticipated by Jones [78]: 'It is quite common for an eigenvalue which is moving steadily towards a positive growth rate to suffer a sudden change of direction and subsequently fail to become unstable; similarly, it happens that modes which initially become more stable as [the Reynolds number] increases change direction and subsequently achieve instability. It is believed that these changes of direction are due to the nearby presence of multiple-eigenvalue points'.

Downloaded from http://rspa.royalsocietypublishing.org/ on September 13, 2017

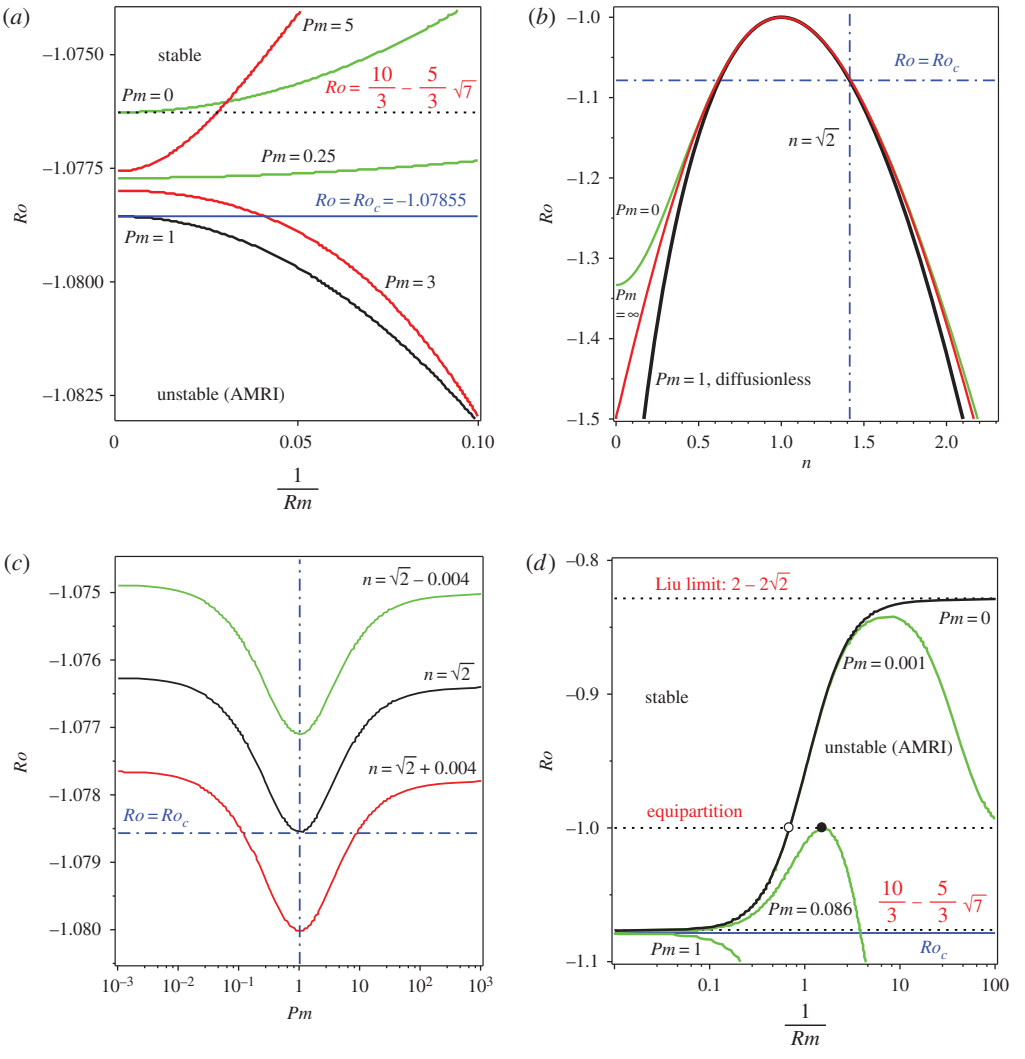

Figure 6. (*a*) For $Rb = -1$, $S = 1$, $n = \sqrt{2}$ and $Re = Rm/Pm$, the neutral stability curves in the (Rm^{-1}, Ro)-plane demonstrating that the limit of the critical value of Ro as $Rm \to \infty$ depends on Pm and attains its minimum Ro_c at $Pm = 1$. (*b*) The limit of the critical value of Ro at $Rb = -1$, $S = 1$ and $Re = Rm/Pm$ as $Rm \to \infty$ plotted as a function of n for (inner curve) $Pm = 1$, (outer curve) $Pm = 0$ and (intermediate curve) $Pm \to \infty$. The limit coincides with the stability boundary of the dissipationless case only at $Pm = 1$, independent of the choice of n. Similarly, at any $Pm \neq 1$ the finite discrepancy between the dissipationless stability curve and the neutral stability curve in the limit of vanishing dissipation exists for all $n > 1$. (*c*) The limit of the critical Ro given by equation (4.5) always has a minimum at $Pm = 1$. (*d*) For $Rb = -1$, $S = 1$, $n = \sqrt{2}$ and $Re = Rm/Pm$, the neutral stability curves at various $Pm \in [0, 1]$ demonstrating that the maximal critical values of Ro do not exceed the Liu limit $2 - 2\sqrt{2}$ that is attained only at $Pm = 0$ in the limit of $Rm \to 0$. (Online version in colour.)

of the critical Rossby number is equal to $\frac{5}{3}(2 - \sqrt{7}) \approx -1.07625 < -1$, i.e. weak dissipation with dominating ohmic losses is not capable to destabilize even the Chandrasekhar equipartition solution at $Ro = -1$. Does the increase in viscosity and resistivity change this tendency?

(ii) AMRI of the Rayleigh-stable flows at low and high *Pm* when dissipation is finite

Indeed, it does. Figure 6*d* demonstrates the evolution of the critical Rossby number as a function of $Rm^{-1} \in [0, 100]$ under the constraint $Rm - RePm = 0$ at various $Pm \in [0, 1]$ in the assumption that $Rb = -1$, $S = 1$ and $n = \sqrt{2}$. Although the critical Rossby number does not exceed the value

Downloaded from http://rspa.royalsocietypublishing.org/ on September 13, 2017

$Ro = -1$ of the equipartition solution for all $Pm \in [0, 1]$ when $Rm^{-1} < 0.1$, it can grow considerably and attain a maximum when $Rm^{-1} > 0.1$. For instance, if $Pm = Pm_l \approx 0.0856058$, the maximal critical value is $Ro = -1$, which is attained at $Rm = Rm_l \approx 0.6552421$ (or $Rm_l^{-1} \approx 1.5261535$); see figure 6*d* where this maximum is marked by the filled circle. For $0 < Pm < Pm_l$, the maximal critical Rossby number exceeds the value of $Ro = -1$.

In the inductionless limit ($Pm = 0$), the azimutal magnetorotational instability (AMRI) occurs at $Ro \geq -1$ if $Rm \leq Rm_*$, where $Rm_* = \frac{1}{2}\sqrt{4 + 2\sqrt{5}}$ ($Rm_*^{-1} \approx 0.6871$, open circle in figure 6*d*). The critical value of the fluid Rossby number monotonically grows with decreasing Rm, attaining its maximal value[8] $Ro^- = 2 - 2\sqrt{2} \approx -0.8284$ at $Rm = 0$.

If $Ro = Rb$, $S = 1$, then at $Pm = 0$ we have

$$Rm_*^2 = \frac{n^2(n^4 - 12Rb^2 + 16Rb) - 16(Rb + 2)(Rb^2 - n^2) - n((n^2 - 2Rb)^2 + 8(Rb^2 - n^2))\sqrt{n^2 + 8Rb + 16}}{32(Rb^2 - n^2)(n^2 - Rb - 2)^2}, \tag{4.6}$$

in agreement with the results of [43]. At $Rb = -1$ and $n = \sqrt{2}$, equation (4.6) yields $Rm_* = \frac{1}{2}\sqrt{4 + 2\sqrt{5}}$.

On the other hand, the lower Liu limit as a function of n and Rb is [43,56]

$$Ro^-(n, Rb) = -2 + (n^2 - 2Rb)\frac{n^2 - 2Rb - \sqrt{(n^2 - 2Rb)^2 - 4n^2}}{2n^2}. \tag{4.7}$$

Note that $Ro^-(n, Rb)$ attains its maximum $2 - 2\sqrt{2}$ at $n = \sqrt{-2Rb}$, which explains our choice[9] of $n = \sqrt{2}$ for the case when $Rb = -1$ (cf. also figure 1*b*). Moreover, at $n = \sqrt{-2Rb}$ the instability condition $Ro < Ro^-$ reduces to (1.11) after some algebra.

We see that there exists a critical value of the magnetic Prandtl number $Pm_l < 1$ such that, at $Pm \in [0, Pm_l]$, the Chandrasekhar equipartition solution with $Rb = Ro = -1$, and $S = 1$ is destabilized by dissipation when viscosity is sufficiently small and ohmic diffusion is sufficiently large. By contrast, at $Ro - Ro_c \ll 1$ the marginally stable diffusionless system can be destabilized at $Pm < 1$ when both viscosity and resistivity are infinitesimally small (figure 4*a*).

To understand how these instabilities are related to each other, we plot the neutral stability curves in the plane of inverse Reynolds numbers $Re^{-1}, Rm^{-1} \in [-0.5, 1]$ for $Ro \in [Ro_c, -1]$ (figure 7*a*). Although negative Reynolds numbers have no physical meaning, it is instructive to extend the neutral stability curves to the corresponding region of the parameter plane. At $Ro = Ro_c$, the stability domain is inside the area bounded by a curve having a cuspidal singularity at the origin with the tangent line at the cuspidal point specified by the condition $Pm = 1$; this geometry yields destabilization by infinitesimally small dissipation at all $Pm \neq 1$.

As soon as Ro departs from Ro_c, the cusp at the origin transforms into a self-intersection, the angle of which increases with the increase in Ro and becomes equal to π at $Ro = -1$. For this reason, at Ro close to -1 the neutral stability curve partially belongs to the region of negative Reynolds numbers which makes destabilization by infinitesimally small dissipation impossible for all $Pm > 0$. In particular, at $S = 1$ and vanishing viscosity the ohmic diffusion is stabilizing in the interval $0 < Rm^{-1} < Rm_*^{-1}$ when

$$Ro > Ro_{Rm} := \frac{6Rb^2 - Rbn^2 + 6n^2 - 2(n^2 - 3Rb)\sqrt{Rb^2 + 3n^2}}{3n^2}. \tag{4.8}$$

At $Rb = -1$ and $n = \sqrt{2}$, we have $Ro_{Rm} = \frac{5}{3}(2 - \sqrt{7}) \approx -1.07625 > Ro_c \approx -1.07855$. At $S = 1$ and $Ro = Rb$, the critical magnetic Reynolds number Rm_* is defined by equation (4.6).

A similar instability domain exists also in the case of $Pm > 1$ (figure 7*a*). At $Ro = -1$, the ray from the origin with the slope $Pm = Pm_u \approx 11.681451$ is tangent to the boundary of the domain at $Re = Re_u \approx 0.6552421$ ($Re_u^{-1} \approx 1.5261535$). In particular, in the case of vanishing ohmic dissipation

[8]Known as the lower Liu limit [43,53,79].

[9]Note that in the recent paper [74], minimization of the Reynolds and Hartmann numbers over n yielded the critical azimuthal wavenumber $n_c \approx 1.4$, which is close to $n = \sqrt{2}$.

Downloaded from http://rspa.royalsocietypublishing.org/ on September 13, 2017

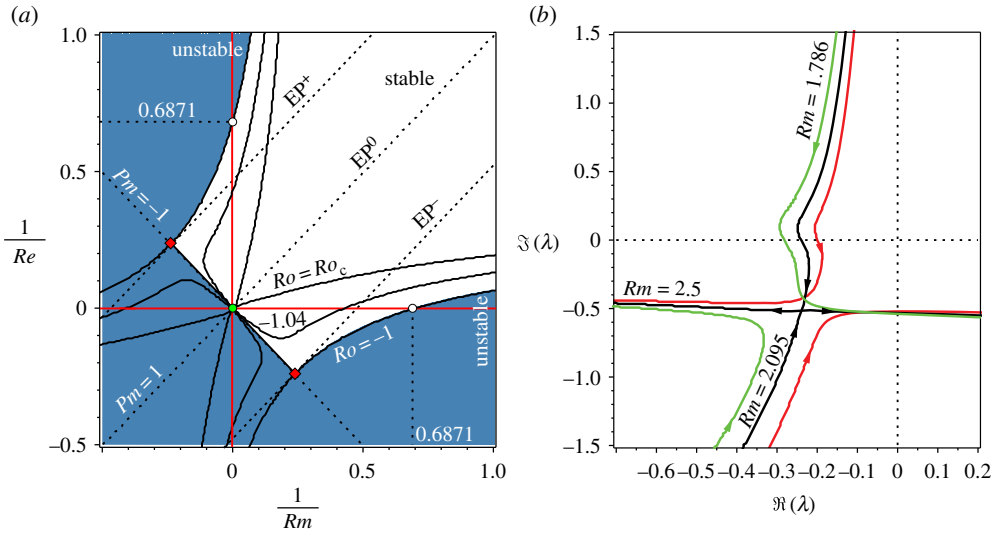

Figure 7. (*a*) Contour plots of the neutral stability surface in the plane of inverse Reynolds numbers at (cuspidal curve) $Ro = Ro_c \approx -1.07855$, (filled area) $Ro = -1$ and (intermediate curve) $Ro = -1.04$. Two singular Whitney umbrella points (filled diamonds) exist at the intersection of the line $Pm = -1$ and the neutral stability curve at $Ro = -1$ and another one exists at the origin when $Ro = Ro_c$. From these singularities lines $EP^{\pm}$, EP^0 of exceptional points are stemming that govern the transfer of modes shown in panel (*b*). (*b*) For $Rb = -1, S = 1, n = \sqrt{2}$ and $Re = 1000$, the movement of eigenvalues with decreasing Ro at various Rm chosen such that $Pm < 1$. At $Rm < 1000$ and up to $Rm = Rm_{EP^-} \approx 2.095$ it is the branch corresponding to perturbed imaginary eigenvalues with positive Krein sign that causes instability. When $Rm = Rm_{EP^-}$, two simple eigenvalues approach each other to merge exactly at $Ro = -1$ into a double eigenvalue whose corresponding matrix is a Jordan block, $\lambda_{EP^-} \approx -\mathrm{i}0.5086 - 0.2391$. At $Rm < Rm_{EP^-}$, the instability shifts to the branch of perturbed imaginary eigenvalues with negative Krein sign. (Online version in colour.)

the instability occurs at $Re < Re_*$ when $Ro > Ro_{Re}$, where Re_* is given by

$$Re_*^2 = \frac{n^6 - 4(Rb+1)n^4 - 4Rb^2(3n^2 + 4Rb + 8) + n(4(Rb+2)^2 - (n^2-2)^2 - 12)\sqrt{n^2 - 8Rb}}{32((Rb+2)^2 - n^2)(n^2 + Rb)^2}. \quad (4.9)$$

At $Rb = -1$ and $n = \sqrt{2}$ we have $Ro_{Re} \approx -1.07639$ and $Re_* = \frac{1}{2}\sqrt{4 + 2\sqrt{5}} = Rm_*$.

Hence, the Chandrasekhar equipartition solution ($Ro = Rb = -1, S = 1$) can be destabilized by dissipation either when $0 \le Pm < Pm_l$ and $0 < Rm < Rm_*$ or when $Pm_u < Pm < \infty$ and $0 < Re < Re_*$, see figure 7*a* where open circles mark the values of Re_* and Rm_*. At $n = \sqrt{2}$, stability of the Chandrasekhar solution is not affected by the double diffusion if $Pm \in [0.0856058, 11.681451]$.

(iii) Transfer of instability between modes when *Pm* significantly deviates from 1

Figure 7*a* shows that the neutral stability curves at $Ro = -1$ orthogonally intersect the anti-diagonal line with the slope $Pm = -1$ at the two exceptional points (marked by the filled diamonds) with the coordinates $(Rm_\diamond^{-1}, -Re_\diamond^{-1})$ and $(-Rm_\diamond^{-1}, Re_\diamond^{-1})$, where

$$Rm_\diamond^{-1} = Re_\diamond^{-1} = \frac{\sqrt{2}}{4n}\sqrt{8n^4 + 20n^2 - 1 - (8n^2+1)^{3/2}}. \quad (4.10)$$

At both exceptional points, there exists a pair of simple imaginary eigenvalues and a double imaginary eigenvalue $\lambda_\diamond$ with a Jordan block:

$$\lambda_\diamond = -\mathrm{i}\frac{4n^2 - 1 - \sqrt{1 + 8n^2}}{4n}. \quad (4.11)$$

Downloaded from http://rspa.royalsocietypublishing.org/ on September 13, 2017

At $n=\sqrt{2}$, equations (4.10) and (4.11) yield

$$Rm_{\diamond}^{-1}=Re_{\diamond}^{-1}=\frac{1}{4}\sqrt{71-17\sqrt{17}}\approx 0.23811 \quad \text{and} \quad \lambda_{\diamond}=-\mathrm{i}\frac{7-\sqrt{17}}{4\sqrt{2}}\approx -\mathrm{i}0.50857. \tag{4.12}$$

A segment of the anti-diagonal between the exceptional points is a part of the stability boundary at $Ro=-1$ and all the eigenvalues at the points of this segment are imaginary.

We see that the domain of asymptotic stability at $Ro=-1$ extends to the region of negative Reynolds numbers and that, at the constraint $Rm=-Re$, the double-diffusive system has imaginary spectrum on the interval between the two exceptional points. If we interpret the negative dissipation as an energy gain, then, formally, we could say that, at $Rm=-Re$, the energy gain is compensated by the energy loss. Non-Hermitian systems in which gain and loss are balanced are known as parity–time (PT) symmetric systems [62,80]. The interval of marginal stability of the PT-symmetric system forms a self-intersection singularity on the stability boundary of a general dissipative system with the Whitney umbrella singularities at the exceptional points corresponding to double imaginary eigenvalues [8,62]. Therefore, the neutral stability surface of our double-diffusive system contains the interval of self-intersection on the Ro-axis ($Ro>Ro_{\mathrm{c}}$) that is orthogonal at $Ro=-1$ to the interval of the anti-diagonal with the slope $Pm=-1$ confined between the two exceptional points. At the exceptional points of this interval and at the exceptional point on the Ro-axis at $Ro=Ro_{\mathrm{c}}$, the neutral stability surface in the (Rm^{-1},Re^{-1},Ro)-space has three Whitney umbrella singularities. The singularities 'hidden' in the region of negative Reynolds numbers are responsible for the separation of domains of AMRI due to weak or strong dissipation.

It turns out that this separation is not only quantitative but also qualitative, as comparison of the movement of eigenvalues demonstrates at fixed $Re=1000$ and $Rm=500$ in figure 5*a* and at $Re=1000$ and $Rm\approx 1.789$ in figure 7*b*. In both cases, $Pm<1$. However, in the case of $Pm=0.5$, it is the branch with lower negative frequencies corresponding to the perturbed imaginary eigenvalues with positive Krein sign of the diffusionless Hamiltonian system that becomes unstable due to prevailing ohmic diffusion. By contrast, at much smaller $Pm\approx 0.001789$ the instability moves to a branch with higher negative frequencies that can be seen as stemming from the imaginary eigenvalues with negative Krein sign of the diffusionless Hamiltonian system. Keeping $Re=1000$ and slightly increasing the magnetic Reynolds number to $Rm\approx 2.095$, we see at $Ro=-1$ the crossing of the eigenvalue branches at the double eigenvalue $\lambda_{EP^-}\approx -\mathrm{i}0.5086-0.2391$. The crossing transforms into another avoided crossing when $Rm=2.5$. At $Rm=2.5$, again, it is the branch corresponding to higher negative frequencies (positive Krein sign) that is destabilized by dissipation (figure 7*b*).

In fact, when $Re=1000$ is given, the branch corresponding to the unperturbed imaginary eigenvalues with positive Krein sign is destabilized by dissipation when the magnetic Reynolds number decreases from $Rm=1000$ ($Pm=1$) to $Rm\approx 2.095$ ($Pm\approx 0.002095$). As soon as $Rm<2.095$ ($Pm<0.002095$), the instability is transferred to a branch corresponding to the unperturbed imaginary eigenvalues with negative Krein sign. The reason is the existence of a set in the stability domain corresponding to double complex eigenvalues. This set exists at $Ro=-1$ and consists of the two straight lines

$$Re^{-1}=\pm 2{Re_{\diamond}}^{-1}+Rm^{-1}, \tag{4.13}$$

that are tangent to the neutral stability curves at the exceptional points with the coordinates $(Rm_{\diamond}^{-1},-Re_{\diamond}^{-1})$ and $(-Rm_{\diamond}^{-1},Re_{\diamond}^{-1})$, where $Rm_{\diamond}$ and $Re_{\diamond}$ are defined by equation (4.10).

In figure 7*a*, the lines corresponding to different signs in equation (4.13) are marked as EP^+ (the upper dot line) and EP^- (the lower dot line). At the points of the EP-lines (4.13), there exist double complex eigenvalues (exceptional points) $\lambda_{\mathrm{EP}^\pm}$ given by the expression

$$\lambda_{\mathrm{EP}^\pm}=\lambda_{\diamond}-(Rm^{-1}\pm Rm_{\diamond}^{-1}). \tag{4.14}$$

Downloaded from http://rspa.royalsocietypublishing.org/ on September 13, 2017

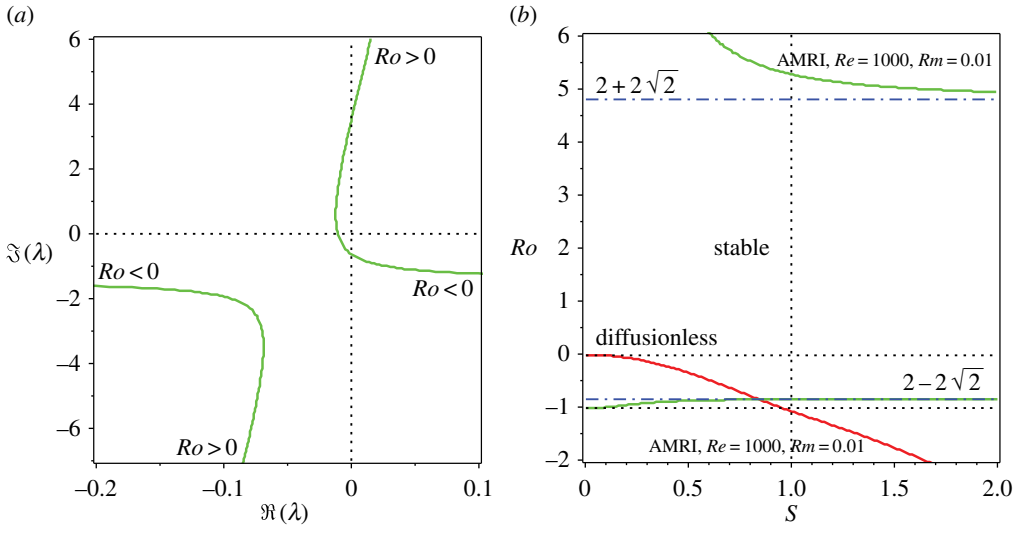

Figure 8. (*a*) For $Rb = -1$, $S = 1$ and $n = \sqrt{2}$, and fixed $Re = 1000$ and $Rm = 0.01$, the movement of eigenvalues in the complex plane as Ro is varied, demonstrating that, at $Pm = 10^{-5}$, one and the same eigenvalue branch is responsible for instability both at $Ro < 0$ and $Ro > 0$. (*b*) The corresponding neutral stability curves in the (S, Ro)-plane exist below the lower Liu limit of $Ro = 2 - 2\sqrt{2}$ (destabilizing the Chandrasekhar equipartition solution) and above the upper Liu limit of $Ro = 2 + 2\sqrt{2}$ that are attainable only at $Re \to \infty$ and $Rm \to 0$. In contrast, the diffusionless AMRI exists above the lower Liu limit at small S but does not affect the Chandrasekhar equipartition solution at $S = 1$. (Online version in colour.)

At $n = \sqrt{2}$ and $Re_{EP^-} = 10^3$, we find that $1/Rm_{EP^-} = 2/Re_\diamond + 1/Re_{EP^-} \approx 0.477$ ($Rm_{EP^-} \approx 2.095$) and

$$\lambda_{EP^-} = \mathrm{i}\frac{\sqrt{17}-7}{4\sqrt{2}} - \frac{1}{4}\sqrt{71 - 17\sqrt{17}} - \frac{1}{Re_{EP^-}} \approx -0.2391 - \mathrm{i}0.5086. \tag{4.15}$$

We see that the three Whitney umbrella points and, related to them, three lines of double complex eigenvalues (marked in figure 7*a* as $EP^{\pm}$ and EP^0) actually control the dissipation-induced destabilization, acting as switches of unstable modes. The singular geometry of the neutral stability surface guides the limiting scenarios and connection of the double-diffusive system to a Hamiltonian or to a PT-symmetric one.

(iv) Connection between the lower and upper Liu limits at $Pm \ll 1$

Let us keep $Re = 1000$ and allow the magnetic Reynolds number to decrease beyond the critical value $Rm_{EP^-} \approx 2.095$. During this process, the pattern of interacting eigenvalues remains qualitatively the same (cf. figures 7*b* and 8*a*). However, an important new feature appears as the magnetic Prandtl number approaches the inductionless limit $Pm = 0$. Indeed, at $Re = 1000$ and $Rm = 0.01$ corresponding to $Pm = 10^{-5}$, one and the same eigenvalue branch has unstable parts both at $Ro < 0$ and at $Ro > 0$ (figure 8*a*). This is in striking contrast to the case of moderately small magnetic Prandtl numbers shown in figure 7*b* or to the diffusionless case when the instability occurs only at $Ro < 0$.

The Bilharz criterion reveals two regions of instability in the (S, Ro)-plane for $Rb = -1$, $n = \sqrt{2}$ and $Re = 1000$ and $Rm = 0.01$ (figure 8*b*). The first one exists at $Ro < 2 - 2\sqrt{2} < 0$ and the second one at $Ro > 2 + 2\sqrt{2} > 0$. In the gap between the lower Liu limit $(2 - 2\sqrt{2})$ and the upper Liu limit $(2 + 2\sqrt{2})$, the system is stable [43,79]. Both Liu limits are attained when $Re \to \infty$ and $Rm \to 0$. If the double-diffusive instability domain at $Ro < 0$ can be considered as a deformation of the instability domain of the diffusionless system, the instability of the magnetized circular Couette–Taylor flow in superrotation [74] at $Ro > 0$ turns out to exist only in the presence of dissipation.

Downloaded from http://rspa.royalsocietypublishing.org/ on September 13, 2017

Remarkably, the two seemingly different instabilities are caused by the eigenvalues living on a single eigenvalue branch in the complex plane (figure 8*a*).

The oscillatory instability at $Pm \ll 1$ of a circular Couette–Taylor flow in an azimuthal magnetic field with $Rb = -1$ and $Ro < 2 - 2\sqrt{2}$, i.e. the AMRI, has already been observed in recent experiments with liquid metals [49]. We therefore identify the observed *inductionless AMRI at* $Pm \ll 1$ *as simply the manifestation of a dissipation-induced instability of waves of negative energy of the diffusionless system caused by the prevailing ohmic diffusion*. In particular, at $Ro = Rb = -1$ and $S = 1$ the inductionless AMRI is the dissipation-induced instability of the Chandrasekhar equipartition solution.

5. Conclusion

We have studied AMRI of a circular Couette–Taylor flow of an incompressible electrically conducting Newtonian fluid in the presence of an azimuthal magnetic field of arbitrary radial dependence. With the use of geometrical optics asymptotic solutions, we have reduced the problem to the analysis of the dispersion relation of the transport equation for the amplitude of a localized perturbation. We have represented the corresponding matrix eigenvalue problem in the form of a Hamiltonian diffusionless system perturbed by ohmic diffusion and fluid viscosity. We have established that the diffusionless AMRI corresponds to the Krein collision of simple imaginary eigenvalues with the opposite Krein (or energy) sign and have derived an analytic expression for the instability threshold of the diffusionless system using the discriminant of the complex polynomial dispersion relation. We have demonstrated that the threshold of the double-diffusive AMRI with equal viscosity and electrical resistivity ($Pm = 1$) smoothly converges to the threshold of the diffusionless AMRI in the limit of the infinitesimally small dissipation, and this result does not change when other parameters are varied.

In contrast with the case when the coefficients of viscosity and resistivity are equal, the prevalence of resistivity over viscosity or vice versa causes the AMRI in the parameter regions where the diffusionless AMRI is prohibited, for instance, in the case of super rotating flows. In particular, non-equal and finite viscosity and resistivity destabilize the celebrated Chandrasekhar energy equipartition solution. Analysing the neutral stability surface of the double-diffusive system, we have found that:

— marginally stable Hamiltonian equilibria of the diffusionless system form an edge on the neutral stability surface of the double-diffusive system that ends up with the Whitney umbrella singular point at the onset of the Hamilton–Hopf bifurcation;
— another edge with the two Whitney umbrella singular points at its ends corresponds to marginally stable double-diffusive systems with the balanced energy gain and loss (PT-symmetric systems);
— three codimension-2 sets corresponding to complex double-degenerate eigenvalues with Jordan blocks (exceptional points) stem from each of the Whitney umbrella singularities and live in the stability domain of the double-diffusive system;
— the sets of exceptional points control transfer of instability between modes of positive and negative energy, whereas the Whitney umbrellas govern the limiting scenarios for the instability thresholds including the case of vanishing dissipation;
— AMRI can be interpreted as an instability of the Chandrasekhar equipartition solution induced by finite dissipation when either $Pm \in [0, 1)$ is sufficiently small or $Pm \in (1, \infty)$ is sufficiently large;
— inductionless AMRI occurring both at $Ro < 0$ and $Ro > 0$ when $Pm \ll 1$ is caused by the eigenvalues of the one and the same branch stemming from the negative energy modes of the diffusionless system, as in the classical dissipation-induced instability.

Data accessibility. This paper has no additional data.
Competing interests. I declare I have no competing interests.

Downloaded from http://rspa.royalsocietypublishing.org/ on September 13, 2017

Funding. Partial support through the EU FP7 ERC grant ERC-2013-ADG-340561-INSTABILITIES is gratefully acknowledged.

Acknowledgements. The author thanks L. Tuckerman and I. Mutabazi for fruitful exchanges on this work.

References

1. Braviner HJ, Ogilvie GI. 2014 Tidal interactions of a Maclaurin spheroid – I. Properties of free oscillation modes. *Mon. Not. R. Astron. Soc.* **441**, 2321–2345. (doi:10.1093/mnras/stu704)
2. Chandrasekhar S. 1984 On stars, their evolution and their stability. *Science* **226**, 497–505. (doi:10.1126/science.226.4674.497)
3. Roberts PH, Stewartson K. 1963 On the stability of a Maclaurin spheroid of small viscosity. *Astrophys. J.* 137, 777–790. (doi:10.1086/147555)
4. Bloch AM, Krishnaprasad PS, Marsden JE, Ratiu TS. 1994 Dissipation-induced instabilities. *Ann. I. H. Poincaré-AN* **11**, 37–90. (doi:10.1016/S0294-1449(16)30196-2)
5. Krechetnikov R, Marsden JE. 2007 Dissipation-induced instabilities in finite dimensions. *Rev. Mod. Phys.* **79**, 519–553. (doi:10.1103/RevModPhys.79.519)
6. Bridges TJ, Dias F. 2007 Enhancement of the Benjamin-Feir instability with dissipation. *Phys. Fluids* **19**, 104104. (doi:10.1063/1.2780793)
7. Kirillov ON, Verhulst F. 2010 Paradoxes of dissipation-induced destabilization or who opened Whitney's umbrella? *Z. Angew. Math. Mech.* **90**, 462–488. (doi:10.1002/zamm.200900315)
8. Kirillov ON. 2013 *Nonconservative stability problems of modern physics*. De Gruyter Studies in Mathematical Physics 14. Berlin, Boston: De Gruyter. (doi:10.1515/9783110270433)
9. Lamb H. 1908 On kinetic stability. *Proc. R. Soc. Lond. A* **80**, 168–177. (doi:10.1098/rspa.1908.0013)
10. Chefranov SG. 2016 Cyclone–anticyclone vortex asymmetry mechanism and linear Ekman friction. *J. Exp. Theor. Phys.* **122**, 759–768. (doi:10.1134/S1063776116040038)
11. Langford WF. 2003 Hopf meets Hamilton under Whitney's umbrella. In *IUTAM symposium on nonlinear stochastic dynamics, Monticello, IL, USA, 26–30 August 2002* (ed. SN Namachchivaya), Solid Mech. Appl. 110, pp. 157–165. Dordrecht, The Netherlands: Kluwer.
12. Holopäinen EO. 1961 On the effect of friction in baroclinic waves. *Tellus* **13**, 363–367. (doi:10.1111/j.2153-3490.1961.tb00097.x)
13. Swaters GE. 2010 Modal interpretation for the Ekman destabilization of inviscidly stable baroclinic flow in the Phillips model. *J. Phys. Oceanogr.* **40**, 830–839. (doi:10.1175/2009JPO4311.1)
14. Willcocks BT, Esler JG. 2012 Nonlinear baroclinic equilibration in the presence of Ekman friction. *J. Phys. Oceanogr.* **42**, 225–242. (doi:10.1175/JPO-D-11-0112.1)
15. Krechetnikov R, Marsden JE. 2009 Dissipation-induced instability phenomena in infinite-dimensional systems. *Arch. Ration. Mech. Anal.* **194**, 611–668. (doi:10.1007/s00205-008-0193-6)
16. Ziegler H. 1952 Die Stabilitätskriterien der Elastomechanik. *Arch. Appl. Mech.* **20**, 49–56. (doi:10.1007/BF00536796)
17. Bottema O. 1956 The Routh-Hurwitz condition for the biquadratic equation. *Indag. Math.* **59**, 403–406. (doi:10.1016/S1385-7258(56)50054-6)
18. Kirillov ON, Seyranian AO. 2005 The effect of small internal and external damping on the stability of distributed non-conservative systems. *J. Appl. Math. Mech.* **69**, 529–552. (doi:10.1016/j.jappmathmech.2005.07.004)
19. Tommasini M, Kirillov ON, Misseroni D, Bigoni D. 2016 The destabilizing effect of external damping: Singular flutter boundary for the Pflüger column with vanishing external dissipation. *J. Mech. Phys. Sol.* **91**, 204–215. (doi:10.1016/j.jmps.2016.03.011)
20. Yih C-S. 1961 Dual role of viscosity in the instability of revolving fluids of variable density. *Phys. Fluids* **4**, 806–811. (doi:10.1063/1.1706410)
21. Turner JS. 1974 Double-diffusive phenomena. *Annu. Rev. Fluid Mech.* **6**, 37–54. (doi:10.1146/annurev.fl.06.010174.000345)
22. Lindblom L, Detweiler SL. 1977 On the secular instabilities of the Maclaurin spheroids. *Astrophys. J.* **211**, 565–567. (doi:10.1086/154964)
23. Ostrovskii LA, Rybak SA, Tsimring LS. 1986 Negative energy waves in hydrodynamics. *Sov. Phys. Usp.* **29**, 1040–1052. (doi:10.1070/PU1986v029n11ABEH003538)
24. Montgomery M. 1993 Hartmann, Lundquist, and Reynolds: the role of dimensionless numbers in nonlinear magnetofluid behavior. *Plasma Phys. Control. Fusion* **35**, B105–B113. (doi:10.1088/0741-3335/35/SB/008)

Downloaded from http://rspa.royalsocietypublishing.org/ on September 13, 2017

25. Thorpe SA, Smyth WD, Li L. 2013 The efect of small viscosity and diffusivity on the marginal stability of stably stratified shear flows. *J. Fluid Mech.* **731**, 461–476. (doi:10.1017/jfm.2013.378)
26. Smith DM. 1933 The motion of a rotor carried by a flexible shaft in flexible bearings. *Proc. R. Soc. Lond. A* **142**, 92–118. (doi:10.1098/rspa.1933.0158)
27. Kirillov ON. 2009 Campbell diagrams of weakly anisotropic flexible rotors. *Proc. R. Soc. A* **465**, 2703–2723. (doi:10.1098/rspa.2009.0055)
28. Acheson DJ, Gibbons MP. 1978 On the instability of toroidal magnetic fields and differential rotation in stars. *Phil. Trans. R. Soc. Lond. A* **289**, 459–500. (doi:10.1098/rsta.1978.0066)
29. Kirillov ON, Mutabazi I. 2017 Short wavelength local instabilities of a circular Couette flow with radial temperature gradient. *J. Fluid Mech.* **818**, 319–343. (doi:10.1017/jfm.2017.99)
30. Rayleigh JWS. 1917 On the dynamics of revolving fluids. *Proc. R. Soc. Lond. A* **93**, 148–154. (doi:10.1098/rspa.1917.0010)
31. Balbus SA, Henri P. 2008 On the magnetic Prandtl number behavior of accretion disks. *Astrophys. J.* **674**, 408–414. (doi:10.1086/524838)
32. Brandenburg A. 2011 Dissipation in dynamos at low and high magnetic Prandtl numbers. *Astron. Nachr.* **332**, 51–56. (doi:10.1002/asna.201011478)
33. Lerner J, Knobloch E. 1985 The stability of dissipative magnetohydrodynamic shear flow in a parallel magnetic field. *Geophys. Astrophys. Fluid Dyn.* **33**, 295–314. (doi:10.1080/03091928508245434)
34. Eckhardt B, Yao D. 1995 Local stability analysis along Lagrangian paths. *Chaos Solitons Fractals* **5**, 2073–2088. (doi:10.1016/0960-0779(95)00016-W)
35. Maeder A, Meynet G, Lagarde N, Charbonnel C. 2013 The thermohaline, Richardson, Rayleigh-Taylor, Solberg-Hoiland, and GSF criteria in rotating stars. *Astron. Astrophys.* **553**, A1–A7. (doi:10.1051/0004-6361/201220936)
36. Balbus SA, Potter WJ. 2016 Surprises in astrophysical gasdynamics. *Rep. Prog. Phys.* **79**, 066901. (doi:10.1088/0034-4885/79/6/066901)
37. Michael DH. 1954 The stability of an incompressible electrically conducting fluid rotating about an axis when current flows parallel to the axis. *Mathematika* **1**, 45–50. (doi:10.1112/S0025579300000516)
38. Kirillov ON, Stefani F. 2013 Extending the range of the inductionless magnetorotational instability. *Phys. Rev. Lett.* **111**, 061103. (doi:10.1103/PhysRevLett.111.061103)
39. Ogilvie GI, Pringle JE. 1996 The non-axisymmetric instability of a cylindrical shear flow containing an azimuthal magnetic field. *Mon. Not. R. Astron. Soc.* **279**, 152–164. (doi:10.1093/mnras/279.1.152)
40. Acheson DJ, Hide R. 1973 Hydromagnetics of rotating fluids. *Rep. Prog. Phys.* **36**, 159–221. (doi:10.1088/0034-4885/36/2/002)
41. Acheson DJ. 1980 'Stable' density stratification as a catalyst for instability. *J. Fluid. Mech.* **96**, 723–733. (doi:10.1017/S0022112080002327)
42. Pearlstein AJ. 1981 Effect of rotation on the stability of a doubly diffusive fluid layer. *J. Fluid. Mech.* **103**, 389–412. (doi:10.1017/S0022112081001390)
43. Kirillov ON, Stefani F, Fukumoto Y. 2014 Local instabilities in magnetized rotational flows: a short-wavelength approach. *J. Fluid Mech.* **760**, 591–633. (doi:10.1017/jfm.2014.614)
44. Chandrasekhar S. 1956 On the stability of the simplest solution of the equations of hydromagnetics. *Proc. Natl Acad. Sci. USA* **42**, 273–276. (doi:10.1073/pnas.42.5.273)
45. Chandrasekhar S. 2010 *A scientific autobiography: S. Chandrasekhar* (ed. KC Wali). Singapore: World Scientific.
46. Golovin SV, Krutikov MK. 2012 Complete classification of stationary flows with constant total pressure of ideal incompressible infinitely conducting fluid. *J. Phys. A: Math. Theor.* **45**, 235501. (doi:10.1088/1751-8113/45/23/235501)
47. Balbus SA, Hawley JF. 1992 A powerful local shear instability in weakly magnetized disks 4. Nonaxisymmetric perturbations. *Astrophys. J.* **400**, 610–621. (doi:10.1086/172022)
48. Bogoyavlenskij OI. 2004 Unsteady equipartition MHD solutions. *J. Math. Phys.* **45**, 381–390. (doi:10.1063/1.1629137)
49. Seilmayer M, Galindo V, Gerbeth G, Gundrum T, Stefani F, Gellert M, Rüdiger G, Schultz M, Hollerbach R. 2014 Experimental evidence for non-axisymmetric magnetorotational instability in an azimuthal magnetic field. *Phys. Rev. Lett.* **113**, 024505. (doi:10.1103/PhysRevLett.113.024505)
50. Monchaux R *et al.* 2007 Generation of a magnetic field by dynamo action in a turbulent flow of liquid sodium. *Phys. Rev. Lett.* **98**, 044502. (doi:10.1103/PhysRevLett.98.044502)

Downloaded from http://rspa.royalsocietypublishing.org/ on September 13, 2017

51. Carle F, Bai K, Casara J, Vanderlick K, Brown E. 2017 Development of magnetic liquid metal suspensions for magnetohydrodynamics. *Phys. Rev. Fluids* **2**, 013301. (doi:10.1103/PhysRevFluids.2.013301)
52. Ji H, Balbus S. 2013 Angular momentum transport in astrophysics and in the lab. *Phys. Today* **66**, 27–33. (doi:10.1063/PT.3.2081)
53. Child A, Kersalé E, Hollerbach R. 2015 Nonaxisymmetric linear instability of cylindrical magnetohydrodynamic Taylor-Couette flow. *Phys. Rev. E* **92**, 033011. (doi:10.1103/PhysRevE.92.033011)
54. Rüdiger G, Schultz M, Stefani F, Mond M. 2015 Diffusive magnetohydrodynamic instabilities beyond the Chandrasekhar theorem. *Astrophys. J.* **811**, 84. (doi:10.1088/0004-637X/811/2/84)
55. Julien K, Knobloch E. 2010 Magnetorotational instability: recent developments. *Phil. Trans. R. Soc. A* **368**, 1607–1633. (doi:10.1098/rsta.2009.0251)
56. Kirillov ON, Stefani F, Fukumoto Y. 2012 A unifying picture of helical and azimuthal MRI, and the universal significance of the Liu limit. *Astrophys. J.* **756**, 83. (doi:10.1088/0004-637X/756/1/83)
57. Morrison PJ, Greene JM. 1980 Noncanonical Hamiltonian density formulation of hydrodynamics and ideal magnetohydrodynamics. *Phys. Rev. Lett.* **45**, 790–794. (doi:10.1103/PhysRevLett.45.790)
58. Ilgisonis VI, Khalzov IV, Smolyakov AI. 2009 Negative energy waves and MHD stability of rotating plasmas. *Nucl. Fusion* **49**, 035008. (doi:10.1088/0029-5515/49/3/035008)
59. Arnold VI. 1972 Lectures on bifurcations in versal families. *Russ. Math. Surv.* **27**, 54–123. (doi:10.1070/RM1972v027n05ABEH001385)
60. MacKay RS. 1991 Movement of eigenvalues of Hamiltonian equilibria under non-Hamiltonian perturbation. *Phys. Lett. A* **155**, 266–268. (doi:10.1016/0375-9601(91)90480-V)
61. Maddocks JH, Overton ML. 1995 Stability theory for dissipatively perturbed Hamiltonian-systems. *Comm. Pure Appl. Math.* **48**, 583–610. (doi:10.1002/cpa.3160480602)
62. Kirillov ON. 2013 Stabilizing and destabilizing perturbations of PT-symmetric indefinitely damped systems. *Phil. Trans. R. Soc. A* **371**, 20120051. (doi:10.1098/rsta.2012.0051)
63. Shalybkov DA. 2009 Hydrodynamic and hydromagnetic stability of the Couette flow. *Phys.-Usp.* 52, 915–935. (doi:10.3367/UFNe.0179.200909d.0971)
64. Kucherenko VV, Kryvko A. 2013 Interaction of Alfvén waves in the linearized system of magnetohydrodynamics for an incompressible ideal fluid. *Russ. J. Math. Phys.* **20**, 56–67. (doi:10.1134/S1061920813010068)
65. Eckhoff KS. 1987 Linear waves and stability in ideal magnetohydrodynamics. *Phys. Fluids* **30**, 3673–3685. (doi:10.1063/1.866404)
66. Lifschitz A. 1991 Short wavelength instabilities of incompressible three-dimensional flows and generation of vorticity. *Phys. Lett. A* **157**, 481–487. (doi:10.1016/0375-9601(91)91023-7)
67. Lifschitz A, Suters WH, Beale JT. 1996 The onset of instability in exact vortex rings with swirl. *J. Comp. Phys.* **129**, 8–29. (doi:10.1006/jcph.1996.0230)
68. Maslov VP. 1986 Coherent structures, resonances, and asymptotic non-uniqueness for Navier–Stokes equations with large Reynolds numbers. *Russian Math. Surv.* **41**, 23–42. (doi:10.1070/RM1986v041n06ABEH004222)
69. Allilueva AI, Shafarevich AI. 2015 Asymptotic solutions of linearized Navier–Stokes equations localized in small neighborhoods of curves and surfaces. *Russian J. Math. Phys.* **22**, 421–436. (doi:10.1134/S1061920815040019)
70. Friedlander S, Vishik MM. 1995 On stability and instability criteria for magnetohydrodynamics. *Chaos* **5**, 416–423. (doi:10.1063/1.166112)
71. Squire J, Bhattacharjee A. 2014 Nonmodal growth of the magnetorotational instability. *Phys. Rev. Lett.* **113**, 025006. (doi:10.1103/PhysRevLett.113.025006)
72. Yakubovich VA, Starzhinskii VM. 1975 *Linear differential equations with periodic coefficients, vols. 1 and 2*. New York, NY: Wiley.
73. Zhang R, Qin H, Davidson RC, Liu J, Xiao J. 2016 On the structure of the two-stream instability–complex G-Hamiltonian structure and Krein collisions between positive- and negative-action modes. *Phys. Plasmas* **23**, 072111. (doi:10.1063/1.4954832)
74. Stefani F, Kirillov ON. 2015 Destabilization of rotating flows with positive shear by azimuthal magnetic fields. *Phys. Rev. E* **92**, 051001(R). (doi:10.1103/PhysRevE.92.051001)
75. Berry MV, Shukla P. 2016 Curl force dynamics: symmetries, chaos and constants of motion. *New J. Phys.* **18**, 063018. (doi:10.1088/1367-2630/18/6/063018)

Downloaded from http://rspa.royalsocietypublishing.org/ on September 13, 2017

76. Andersson N. 2003 Gravitational waves from instabilities in relativistic stars. *Class. Quantum Grav.* **20**, R105–R144. (doi:10.1088/0264-9381/20/7/201)
77. Bilharz H. 1944 Bemerkung zu einem Satze von Hurwitz. *Z. Angew. Math. Mech.* **24**, 77–82. (doi:10.1002/zamm.19440240205)
78. Jones JA. 1988 Multiple eigenvalues and mode classification in plane Poiseuille flow. *Quart. J. Mech. Appl. Math.* **41**, 363–382. (doi:10.1093/qjmam/41.3.363)
79. Liu W, Goodman J, Herron I, Ji H. 2006 Helical magnetorotational instability in magnetized Taylor-Couette flow. *Phys. Rev. E* **74**, 056302. (doi:10.1103/PhysRevE.74.056302)
80. Schindler J, Li A, Zheng MC, Ellis FM, Kottos T. 2011 Experimental study of active LRC circuits with PT symmetries. *Phys. Rev. A* **84**, 040101(R). (doi:10.1103/PhysRevA.84.040101)